INTEGRATED GEOPHYSICAL TECHNIQUES FOR GROUND WATER POTENTIAL EVALUATION IN MATUU: MACHAKOS COUNTY, KENYA.

EVANCE ODERO OBONYO

MASTER OF SCIENCE

(Applied Geophysics)

JOMO KENYATTA UNIVERSITY OF AGRICULTURE AND TECHNOLOGY

2016

Integrated Geophysical Techniques For Ground Water Potential Evaluation In Matuu: Machakos County, Kenya.

Evance Odero Obonyo

A Thesis Submitted in Fulfillment for the Degree of Master of Science in Applied Geophysics in the Jomo Kenyatta University of Agriculture and Technology.

2016

DECLARATION

This thesis is my original work and has not been presented for a degree in any other university.

Signature…… Date……..

Evance Odero Obonyo

This thesis has been submitted for examination with our approval as university supervisors.

Signature…….. Date…….

Dr. K'Orowe Maurice

JKUAT, Kenya

Signature…….. Date……

Dr. Githiri Gitonga

JKUAT, Kenya

DEDICATION

I dedicate my entire work to God Almighty.

ACKNOWLEDGEMENT

First, is a sincere thanksgiving to God Almighty for his never failing strength in times of need, all that is in this work is not by human might but by enabling power from Him, without Him I believe nothing much could be achieved.

Secondly, I sincerely thank my supervisors, Dr. K'Orowe and Dr. Githiri of department of physics, Jomo Kenyatta University of Agriculture and Technology for meticulous guidance through the comprehensive stages of research and ensuring a steady scientific growth in me to this end. Through understanding, they managed to transform weaknesses into strengths and sacrificially enabled me to achieve research objectives.

Thirdly, Society of Exploration Geophysicist (SEG) Foundation through the JKUAT Chapter played a pivotal role in providing practical experiences on geophysical exploration where a number of techniques among which this research employed were practiced through sponsored field camp. Moreover, they financially supported this research and it is for these reasons that I give my heartfelt gratitude. I extend this gratitude to all members of SEG, JKUAT Chapter for the time and comfort sacrificed for my field work more so to Mr. Munyithya for his logistical support throughout the field work period.

I owe special thanks to Mr. Methusela of World Vision, Matuu, and Ministry of Water and Irrigation in conjunction with TanArthi Water Services for making available hydrogeological reports/borehole logs I needed for this research in time. Thanks to the

county government of Machakos for ensuring security within and around the study area and harmonious association with the locals.

I appreciate the role my family and siblings have played during the study time. They may not have realized that their high expectation has propelled this work making it take relatively short time. Friends have ever supported me throughout with their constant motivation and this deserves applause.

Finally, I would like to appreciate JKUAT Administration through the Department of Physics for providing good research environment, equipment and logistical support.

TABLE OF CONTENTS

LIST OF TABLES

LIST OF FIGURES

LIST OF APPENDICES

ABBREVIATIONS AND ACRONYMS

2D	Two Dimensional
3D	Three Dimensional
CST	Constant Separation Traversing
DC	Direct Current
EMBS	Eastern Mozambique Belt Segment
HG	Horizontal Gradient
IGRF	International Geomagnetic Reference Field
nT	nanotesla
SP	Self-Potential
VES	Vertical Electrical Sounding
Alt	Altitude

LIST OF SYMBOLS

A	Anisotropy
Ω	Ohm
F	Force
r	Separation distance
μ_0	Magnetic permeability of vacuum
μ_R	Magnetic permeability of medium
π	pi
m	Magnetic pole
B	Magnetic field
H	Magnetic North component
Z	Vertical component of magnetic field
I	Inclination angle of geomagnetic field
α	Declination angle of geomagnetic field
Δ	Delta
k	Susceptibility
L	Half current electrode separation
l	Half potential electrode separation
ρ_a	Apparent resistivity
d	Depth
h	Aquifer thickness
S	Siemens
K	Hydraulic conductivity

T	Transmissivity
R	Transverse resistance
S_L	Longitudinal conductance
N	Number of layers of geo-electric section
e	Exponent
x, y, z	Position coordinates
$\approx$	Almost equal to
$\leq$	Less than or equal to
$\geq$	Greater than or equal to
$>$	Greater than
$<$	Less than

ABSTRACT

Matuu-Kilango area in Yatta is fall in an arid area with high rate of evaporation its rivers are dry for the better part of the year, there is therefore need to help identify alternative sources that include underground water for domestic and agricultural use. This study was aimed at evaluating groundwater potential of Matuu-Kilango area in Yatta District using integrated geophysical techniques so as to eliminate borehole failures associated with lack of proper techniques for siting boreholes. Resistivity and magnetic geophysical techniques supported by borehole logs were used to delineate subsurface fluid conduits and determine aquifer characteristics. For magnetic survey, Geometrics 856 Proton Precession Magnetometer was used, 189 measurement points were established, data subjected to corrections and upon processing, disjointed formations revealed by Euler plots under magnetic anomalous area led to inference of a fault in the NW-SE direction to the west of study area. Wenner and Schlumberger arrays were applied in Resistivity survey; Grids were established in the 25 Km^2 area within which 11 measurement stations were located. Apparent resistivity data obtained from Wenner array measurements were subjected to contour plotting using Surfer 10 software with contour interval of 10 Ωm, VES data from the 11 stations were subjected to digital inversion using IPI2Win software, geo-electric parameters were calculated. Data averages from self-potential measurements were analysed as well as transmissivity attributes of the aquifer zones of the study area. Integrating the results, groundwater potential indicators (primers) such as fault, fractures, low resistivity layer (approximately 130 Ωm), negative self-potential zone with ranges between -10 mV to -90 mV, average transmissivity value

of 10 m^2/day and an inferred aquifer, were found to characterize the western zone of Matuu-Kilango area. The aquifer had a lateral stretch of about 1500 metres, a depth of about 100 meters and thickness ranging from 10 metres to about 80 metres northwards. A conceptual model for Matuu-Kilango groundwater potential zone was developed showing the north western part of the study area as the best zones for siting bore holes.

CHAPTER ONE

INTRODUCTION AND LITERATURE REVIEW

This chapter outlines the introductory aspects of the study such as the background of the study, topographical information of Matuu-Kilango area as well as its geological and structural setting. A review of literature on previous related work together with theoretical concepts of all applied techniques on data collection, processing and analysis is covered in this chapter together with statement of research objectives, problem and justification.

1.1 Background of the study

Climate change and global warming are the main causes of unreliable rainfall. This has been the main cause of water shortage leading to severe drought especially in arid and semi-arid areas. Groundwater has successfully been used as alternative means of water supply where rainfall is scarce (Olorunfemi & Fasuyi, 1993). Groundwater potential basically refers to the ability of subsurface at a given geographical area to hold underground water resource; this water occurs in pore spaces between mineral grains or in fractures in a rock mass (Gangadhara, 1992). Crystalline rock comprise of compacted hard rocks such as granite and metamorphic rocks within which occurrence of groundwater is limited to the existence of weathered and fractured zones, this concept was verified by a study in the sub-Saharan crystalline hard rock system by MacDonald, Davis & O'Dochartaigh (2001); a geological setting similar to that of Matuu-Kilango

area. However, losses associated to borehole failure have been incurred in an attempt to site ground water resources without sufficient information from surface exploration using geophysical techniques.

Hard rock system poses a complex situation for groundwater potential evaluation therefore a proper understanding of its hydrogeological characteristics is necessary. It has been proven that geophysical methods are the most reliable and accurate subsurface structural investigation method, Amarachi and Ako (2012), this become even better when the techniques are integrated. This study being an integrated survey incorporated electrical resistivity technique with Schlumberger and Wenner arrays together with magnetic technique. The measurements involved helped locate best zones where bore holes with good yields can be sited guided by the information about primers; faults, fractures, self-generated electric potential trends in the subsurface, surface river patterns and other geological/physical features that define an aquifer. Logging information on available bore holes was also used to constrain the survey data so as to arrive at a conclusive report on the available groundwater resource.

Among the surface geophysical techniques, the electrical resistivity method is widely used. Geophysical methods such as magnetic-induced polarization and electromagnetic methods are secondary and useful to identify the presence of structural discontinuities and intrusive bodies of geological origin. However, in crystalline rocks, exploration by these electromagnetic methods is not highly successful (Murty & Raghavan, 2002). In

this research, the utility of the electrical resistivity method was supported by information from magnetic method for conclusive groundwater evaluation in Matuu, Kenya.

Magnetic survey involves measurement of total magnetic field. Magnetic anomaly is a variation from known earth's magnetic field; it is classified as high if the measured field value is higher than the globally predicted value and low if the measured field value is lower. The aim of a magnetic survey is to investigate subsurface geology on the basis of the anomalies in the earth's magnetic field resulting from the magnetic properties of the underlying rocks. In general, the magnetic susceptibility of rocks is extremely variable depending on the type of rock and the environment it is in. Common causes of magnetic anomalies include dykes, faults and lava flows (Mariita, 2009). In this survey the technique was useful in mapping out faults and fractures which are the major water conduits.

1.1.1 Study area

Matuu-Kilango area is located in Yatta District, Machakos County approximately 110 km from Nairobi, 61.69 km from Thika town. The study area is bounded by latitudes 1^{o} 05'S (9879000 metres) and 1^{o}08'S (9874000 metres) and Longitudes 37^{o} 31'E (335000 metres) and 37^{o} 33'E (340000 metres), zone 37M as illustrated in the figure 1. The area lies along the Eastern Mozambique Belt segment (EMBS) which stretches in our country (Kenya), about 800 km length and 200 km width at 3^{0}N and 4^{0}S latitudes and between 37^{0}E and 39^{0}E longitudes (Mathu, 1992). In the study area, the surface rocks comprise of Metamorphic rocks which are overlain by the Yatta Plateau to

the south. Matuu area is entirely underlain by Precambrian rocks of the basement system. The area of interest is located in Eastern side of Gregory Rift Valley. The area is largely semi-arid characterized by unreliable rainfall; moreover, given that the area is majorly made up of igneous rock formations its porosity is mainly secondary. The future of ground water exploration is of great interest and importance to economic growth. Thus Matuu area to the North was assessed using integrated methods to investigate geo-physical formations of the ground and characterize ground water aquifers.

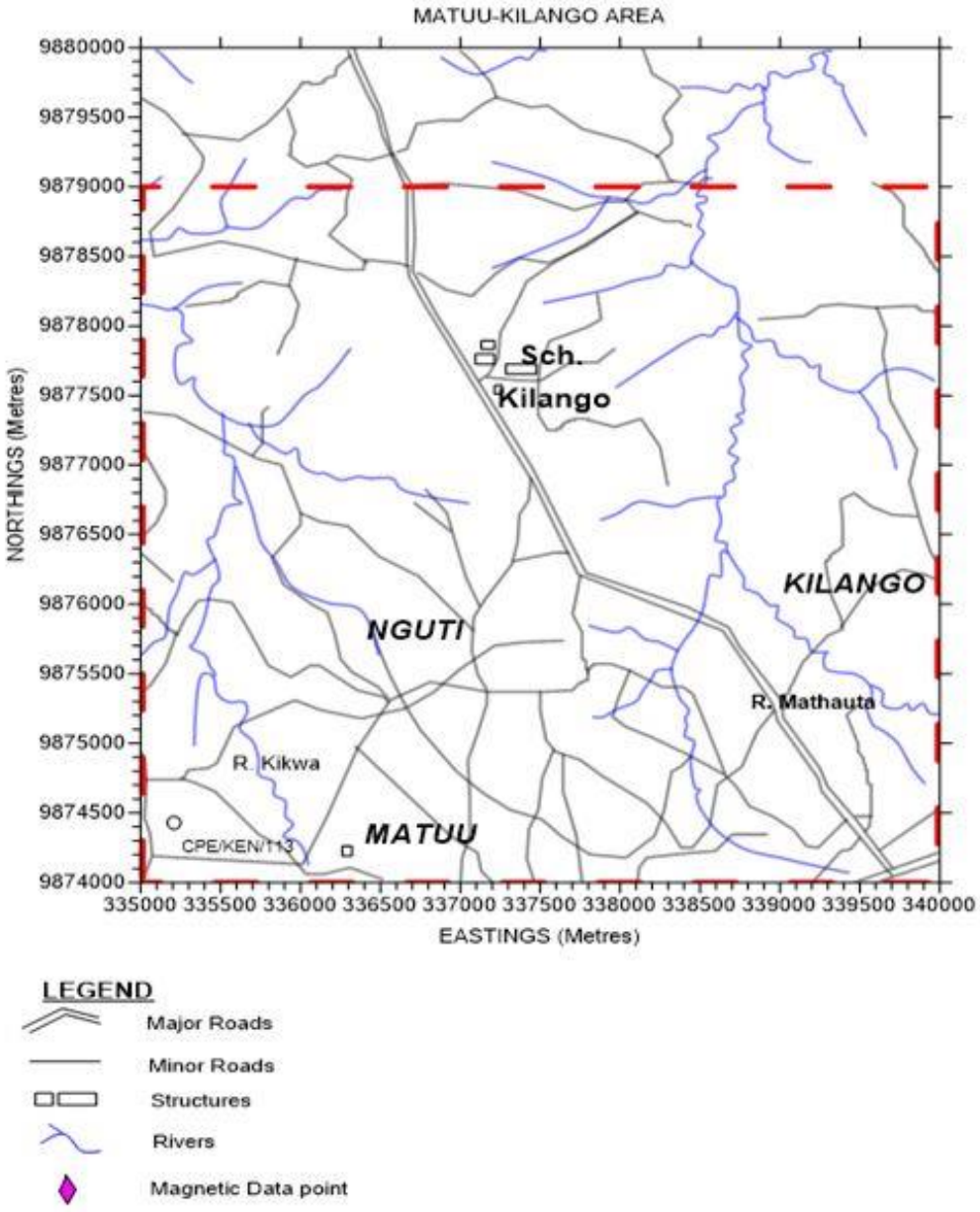

Figure 1: Map of Matuu-Kilango, dashed boundaries shows study area, (Adapted from Survey of Kenya, 2005)

1.1.2 Geology of Study Area

The study area is located in the Eastern side of Gregory Rift valley. Prior to the formation of the Rift valley, the whole area was characterized by Precambrian basement crystalline rock system of Mozambique belt segment (EMBS) which stretches in Kenya about 800 km length and 200 km width at 3^0N and 4^0S latitudes and between 37^0E and 39^0E longitudes as shown in figure 2 (Mathu, 1992). These rocks have undergone through cycle of metamorphism, exposure and erosion. The surface rocks comprises of metamorphic rocks overlain by a Plateau (Yatta) to the south, the formation of Yatta plateau begun at the start of Miocene period by eruption of Phonolites. This resulted into large part sub-Miocene surface being covered by lava. This geological system only hold water in a network of fractures and faults since the metamorphic rocks are non-porous and impervious. The study area is enclosed within the zone II shown in figure 2 and is described by meta-intrusive mafic and ultramafic rocks that include Diorites, Gabbros, Anorthosites, Peridotites and Picrites. The mafic and ultra-mafic rocks occur in the general machakos area and its environs (Nyamai, Mathu, Opiyo-Akech & Wallbrecher , 2003). The study area (Matuu-Kilango) is largely semi-arid.

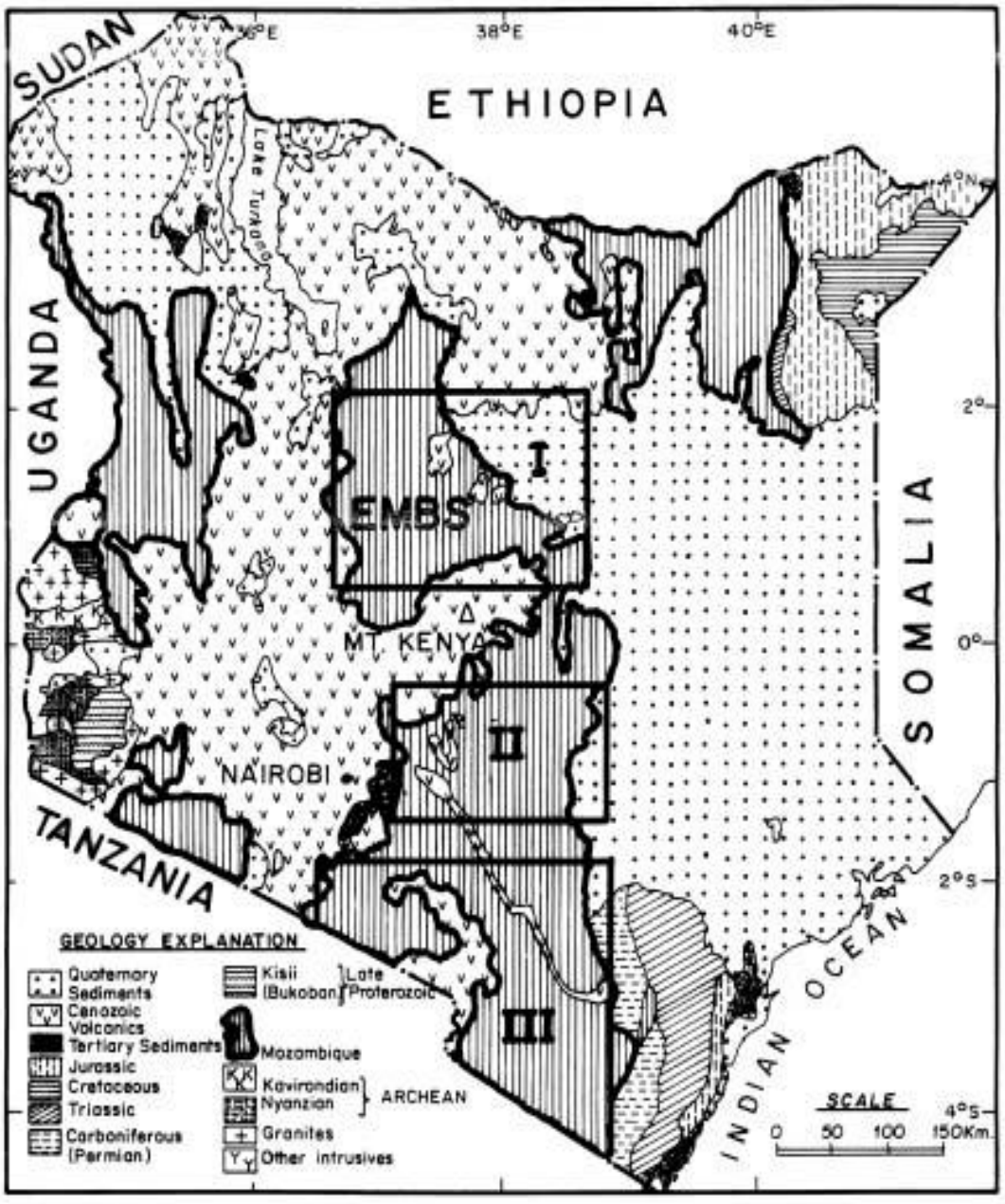

Figure 2: General Geological map of Kenya showing the Eastern Mozambique Belt Segment (Nyamai et al., 2003)

1.1.3 Structural setting of Study area

Major folds with axial traces of tens of kilometers by length are common in the EMBS including zone II and about three fold generations have been distinguished in various sections of the belt (Nyamai, Opiyo-Akech, Gaciri, & Fujimaki, 1999). In the central zone II (Figure 2), the Matuu-Kilango area and the North, the superposed folds have formed elliptical to refolded structural domes and basin whose cores have been interpreted to be the sites occupied by granites and granitoid circular domes (Baker, 1963; William, 1966; Nyamai et al., 1999).

Figure 3 adopted from Mosley (1993) shows how Mutito fault/shear zone and south-westerly located Yatta shear zone have segmented the EMBS into distinct structural or tectonic units (at least three). The three major tectonic domes have been referred to as the Eastern, the Central and the Western domains (Nyamai et al., 2003). The area of study lies within the central domain. In the eastern and central domains lineations are north-west to north-south oriented parallel to the shear zones (Mosley, 1993), inferred brittle/ductile fractures oriented in the North-West and South-East directions are found within the domain (Figure 3). Thrust faults are fewer in the central domain but abundant in the southern zone III and northern zone I (Figure 3). Mulwa, Gaciri, Barongo, Opiyo-Akech, and Kianji (2005) suggested that the best faults i.e. those that form excellent aquifers, are filled with weathered materials and boreholes sunk at these zones have high yield. However, faults filled with impermeable materials act as barriers to the flow of groundwater. These are part of the key parameters considered in this survey. The map

(Figure 3) equally shows a stretch of Yatta Plateau characterized by stretching lineations at the south-western side of the study area.

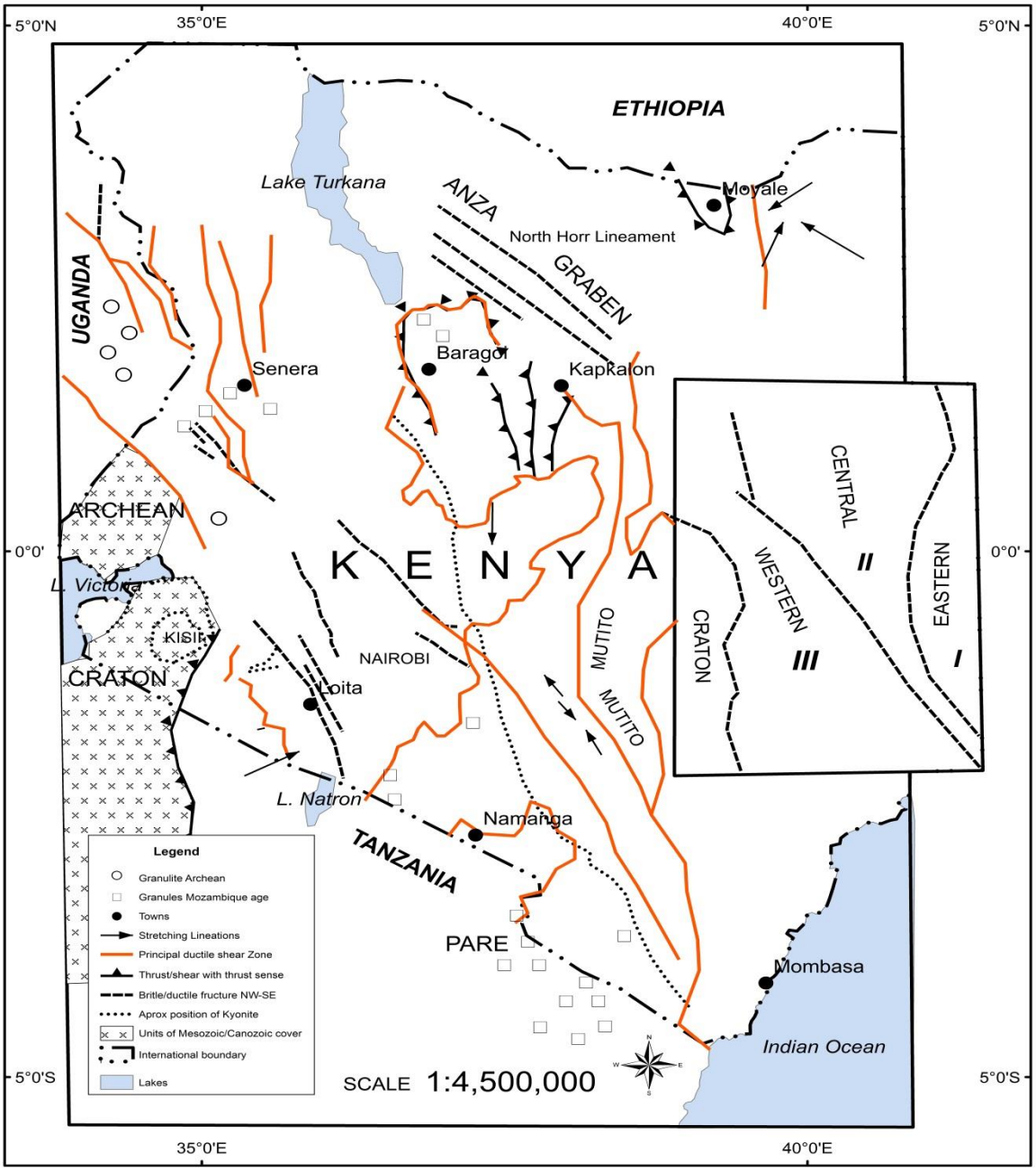

Figure 3: Principal geological structures (Mosley, 1993)

1.2 Literature Review

The process for evaluating ground water potential begins with application of geophysical techniques to delineate hydrogeological features that are groundwater primers. Work done by Sharma and Baranwal (2005) indicated that size, location, interconnection, clogging of fractures together with recharging sources determines viability of ground water resource and how much water can be drawn from it. If these factors are not clearly considered high rate of borehole failures can be registered. This therefore demands for integrated measurements and a number of control measures in data analysis.

Anudu, Onuba, and Ufond (2011) utilized resistivity method (VES) in an area dominated by banded gneiss and quartzite rocks at Onipe in Nigeria. They reported four distinct geo-electrical layers with fractured layer defining the aquifer bounded between a resistive top layer and a basement. A related study carried out by K'Orowe, Nyadawa, M., Singh, V. and Rangarajan (2012) from a typically hard rock terrain found in the Jangaon sub-watershed, Andhra Pradesh, India, showed linear relationship between transmissivity and formation factor by employing resistivity method. Utom, Odoh, & Okoro (2012) established a working relationship between transmissivity and longitudinal conductance of Enugu town in Nigeria as an attempt to evaluate groundwater potential of the zone. The resistivity method is effective in characterizing fracture orientation in shallow bedrock environment (Bills, Truini, Flynn, Pierce, Catchings, & Rymer, 2000). Melinda, David, Michael, and Todd (1997) applied the resistivity method to characterize crystalline rock aquifer at Georgia. In evaluation of borehole failures at Kaduna State, Nigeria, Afuwai, Lawal, Sule, & Ikpokotne (2014) utilized the VES technique

successfully. Properly conducted and interpreted VES by Das, Mondal, and Singh (2007), in hard rock zones of Vizianagaram district in Andhra Pradesh, India resulted into 42 boreholes with yields ranging from 1500-1800 liters per hour. Mogaji, Olayanju, and Olalapo (2011), applied deep electrical soundings to map geo-electric sections across various rock types in the basement complex areas of Ondo State, South-Western Nigeria and developed a typical model of subsurface layers with an aim of aquifer identification and characterization. Compiled report of work done in Hyderabad, India by Ahmed, Jayakumar, and Salih (2008) on geophysical characterization of Hard Rock Aquifers verified that draw down in a bore-well is often almost equal to the total saturated thickness of the aquifer. Schlumberger technique employed by Lateef, (2012) was pivotal in mapping aquiferous zone which was found to be at a depth of about 30 meters within the complex basement of Ekiti State, Nigeria.

Magnetic survey, using Proton precession magnetometer, is a total field measurement technique (Keary, Brooks, & Hill, 2002; Telford, Geldart, & Sheriff, 1990). A study conducted at northern part of Wadi Fatima in Saudi Arabia by Mansour, (2009) for groundwater exploration where magnetic technique was instrumental in delineating basement structures which control ground water flow. Magnetic technique is not directly applied to ground water, since water has no magnetic properties, but greatly used in subsurface geology for mapping rock susceptibilities (Mariita, 2009). This helps indicate zones of discontinuities thus providing a guide on where to apply DC resistivity deep sounding for the potentiality of ground water occurrence. With Olkaria field in Kenya as case study, Mariita, (2009) explained the use of magnetic survey to delineate faults and

heat sources for geothermal exploration. Magnetic profile carried out in Maheswaram waterwashed exposed a dyke by monitoring vertical gradients of Earth's magnetic field (Ahmed et al., 2008). Moreover, horizontal gradient analyses equally apply in magnetic data analysis as utilized by Setyawan, Yudianto, Nishijima, and Hakim (2015), in mapping the faults of Gedongsongo geothermal field of Indonesia. Reynolds, (1998), states that magnetic data interpretation needs to be correlated to other geophysical techniques. Automatic methods have been applied to interpret magnetic data, for example, magnetic data obtained over western continental margin of India by Pawan, Ramprasad, Ramana, Desa, and Shailaja (2007), were subjected to Euler Deconvolution and result obtained showed sharp basement rise at the center of study region governed by Precambrian tectonics.

Mathu, (1992) carried out geological work covering the Matuu area and the surrounding and indicated that from eruption of Yatta Phonolites in the Miocene period the rocks have undergone cycle of metamorphism, exposure and erosion leading to surface rocks comprising of metamorphic rocks of granitic origin.

Within then study area only one out of four boreholes is reported to have attempted the use of resistivity survey to arrive at the drilling site, this happened to be the only method applied in this case, the borehole was successful and still in use to date (Ndeto, 2011).

The survey integrated several arrays of DC-Resistivity method together with ground magnetic techniques to identify ground water primers, characterize the survey region geophysically based on the structural information obtained and establish aquifer geometry.

1.3 Theoretical Concepts

1.3.1 Magnetic Method

The aim of magnetic survey is to investigate subsurface geology on the basis of anomalies in the Earth's magnetic field due to magnetic properties of the subsurface geological features. The survey can be performed at sea, in the air and on land. These features are defined by magnetic poles as a consequence of their magnetic properties. The force (F) between two magnetic poles of strengths m_1 and m_2 separated by distance r is given by equation 1, (Keary et al., 2002).

$$F = \frac{\mu_0 m_1 m_2}{4\pi\mu_R r^2} \quad \ldots\ldots 1$$

Where μ_0 and μ_R are magnetic permeability of vacuum and relative magnetic permeability of medium separating the poles respectively.

The magnetic field B due to the pole of strength m at the same distance is defined by equation 2, (Keary et al., 2002).

$$B = \frac{\mu_0 m}{4\pi\mu_R r^2} \quad \ldots\ldots 2$$

Where μ_0 and μ_R are magnetic permeability of vacuum and relative magnetic permeability of medium separating the poles respectively.

Magnetic field has elements or components in the north direction (H), vertical component (Z) and resolved value giving the total field (B) (Figure 4 (a)). Describing the geomagnetic field elements by vectors, the relationship in equation 3 is obtained.

$$B^2 = H^2 + Z^2 \quad \text{..... 3}$$

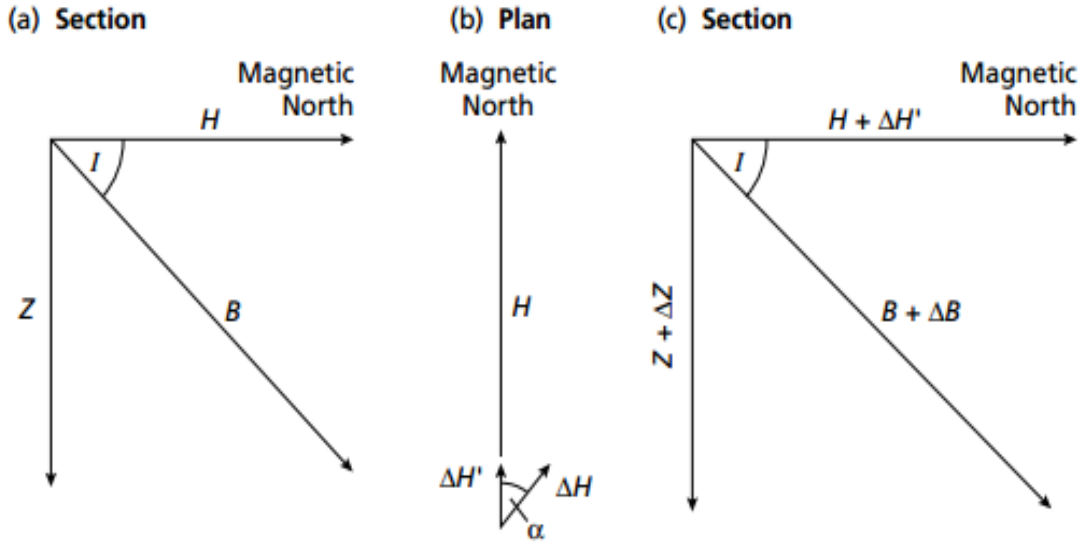

Figure 4: The relationship of magnetic components, (a) section for elements (b) plan for magnetic north (c) plan showing changes in the elements (Keary et al., 2002)

The anomaly will create a change (ΔB) on total field with vertical component (ΔZ) and horizontal component (ΔH) as shown in figure 4(c) from the geomagnetic values B, Z and H respectively, leading to equation 4 by vector relations. Introducing angular descriptions and component relations and taking Δ^2 values as insignificant, equation 5 can be developed from equation 4 with I as the inclination of geomagnetic field.

$$(B + \Delta B)^2 = \left(H + \Delta H^{'}\right)^2 + (Z + \Delta Z)^2 \quad \text{..... 4}$$

$$\Delta B = \Delta Z \sin I + \Delta H \cos I \cos \alpha \quad \text{.....5}$$

Taking $\mu_R = 1$, small isolated positive pole $(+m)$ located at depth z and x as the horizontal distance from observation point, the horizontal (ΔH), vertical (ΔZ) and total field (ΔB) anomalies due to an isolated positive pole arise and the expression for these anomalies given by equations 6 and 7 can be developed from equation 1,. Figure 5 shows magnetic anomaly curves due to isolated body of magnetic strength m with trend of variation in vertical, horizontal and total field components as the observation point change along magnetic north direction.

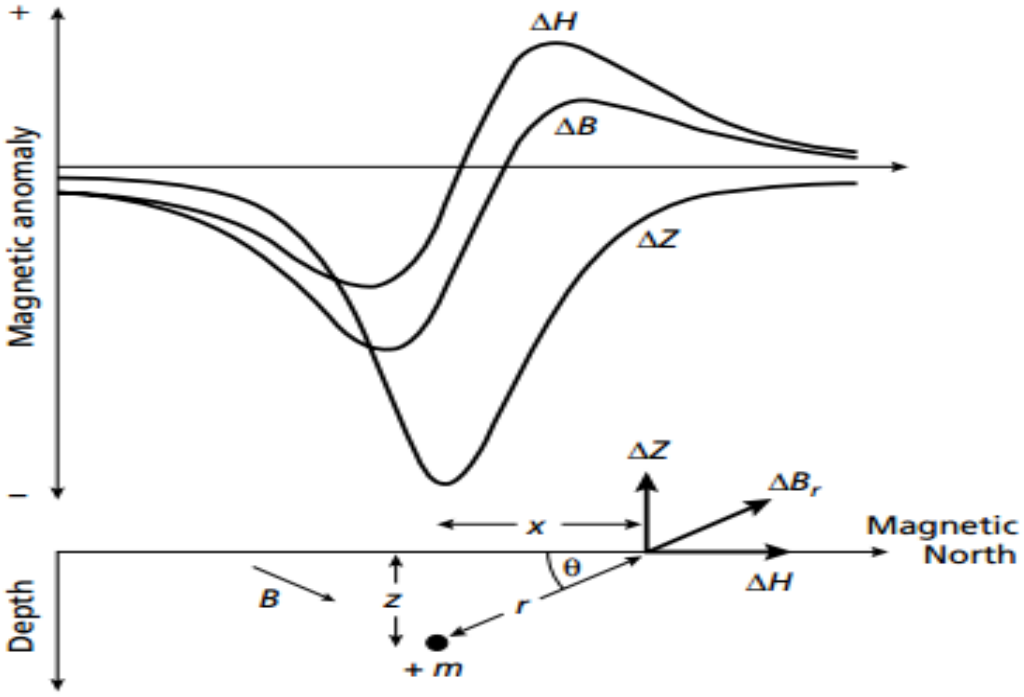

Figure 5: The magnetic anomaly curves, (Keary et al., 2002)

The total field anomaly (ΔB) is then obtained by equations 6 and 7 substituted in equation 5 with $\alpha = 0$ (profiles taken in the direction of magnetic north).

$$\Delta Z = \frac{-\mu_0 mz}{4\pi r^3} \qquad (6)$$

$$\Delta H = \frac{\mu_0 mx}{4\pi r^3} \qquad (7)$$

Equation 8 defines the anomaly and which is related to susceptibility (k) as shown by equation 9;

$$\Delta B = \frac{-\mu_0 mz}{4\pi r^3}\sin I + \frac{\mu_0 mx}{4\pi r^3}\cos I \qquad (8)$$

$$\mu_0 = \frac{\mu}{k+1} \qquad (9)$$

1.3.1.1 Diurnal Variation and Magnetic Storms

The daily changes in the Earth's magnetic field are referred to as *diurnal variations.* The changes are due to changes in the strength and direction of currents in the ionosphere. The effect is estimated to be in the order of 50 nT with maximums at the geomagnetic equator (Reynolds, 1998). The changes are least at night and maximum a few hours after mid-day. However, rapid onsets of fluctuations in the order of hundreds/thousands of nanoteslas are called *magnetic storms.* These are caused by sunspot and solar activities. The magnetic storms, unlike diurnal variation, can lead to termination of survey process since they are difficult to correct for. The diurnal effect can be corrected for by occupying a base station regularly visited during a day's survey (Telford et al., 1990)

1.3.1.2 2D-Euler Deconvolution Technique

Other than Peter's Half-Slope method of subsurface depth estimations, Euler deconvolution method is a more precise alternative since it operates on data directly and provide mathematical solutions without recourse to any geological constrains thus best for structural interpretations (Reynolds, 1998). By use of structural indices related to different magnetic sources and gradient of total magnetic field, Euler's equation (Eq. 10) can be applied accurately to determine depth estimates of the sources.

$$(x-x_0)\frac{\partial T}{\partial x}+(y-y_0)\frac{\partial T}{\partial y}+(z-z_0)\frac{\partial T}{\partial z}=N(B-T)\ldots\ldots\ldots\ldots\ldots\ldots\ldots\ldots\ldots\ldots 10$$

where x_0, y_0, z_0 are the coordinates of magnetic source whose total field intensity T and regional value B are measured at position defined by x, y, z with N as degree of homogeneity (structural index) (Keary et al., 2002).

In two dimensional cases, as for magnetic anomaly, the equation has only two unknowns x_0 and y_0 to be evaluated since N is theoretically known. N ranges between 0 and 1 is best for fault by magnetic method as suggested by Grauch, Hudson, Minor, and Caine (2006). Regions of clustered Euler solutions with discontinuities are normally of interest when delineating faults (Githiri, Patel, Barongo, & Karanja, 2011)

1.3.1.3 Horizontal Gradient

Horizontal gradient technique is a tool for analysing magnetics and gravity data. It is useful in imaging subsurface structures for various applications. The greatest advantage

of horizontal gradient method is that it is least susceptible to noise in the data and only requires calculation of two first-order horizontal derivatives as shown in equation 11.

$$HG(x,y)=\left[\left(\frac{\partial H}{\partial x}\right)^2+\left(\frac{\partial H}{\partial y}\right)^2\right]^{1/2} \quad \text{.....} \quad 11$$

Where $\left(\frac{\partial H}{\partial x}\right)$ and $\left(\frac{\partial H}{\partial y}\right)$ are horizontal derivatives of magnetic field in x and y directions, (Setyawan et al., 2015).

Horizontal gradient method applied in mapping faults is able to delineate subsurface faults that have no evidence on the surface and are associated to high horizontal gradient anomalies interpreted as boundaries or faults, (Setyawan et al., 2015). Githiri et al., (2011), explains that horizontal gradient analysis applied to 2D magnetic situations tend to place narrow ridges over abrupt changes in magnetization and this can be inferred by simple inspection.

1.3.2 Resistivity Method

Here electric current is injected into the ground leading to potential differences which deviate in a pattern depending on the subsurface conducting bodies or inhomogeneity. Based on the objective of a given survey, several configurations can be realized.

1.3.2.1 Electrical Self-Potential

Self-potential (SP) or Spontaneous polarization are potential differences resulting from natural subsurface processes e.g. groundwater movement, streaming fluids, and other

subsurface geochemical reactions, (Keary et al., 2002). The common factor among the various processes thought to be responsible for measured self-potentials is groundwater acting as electrolyte and solvent of different minerals. Moreover, negative self-potential values below -100mV is associated with groundwater, (Jinadasa & Silva, 2009; Reynolds, 1998).

For a mineral body, large negative anomalies, normally above -100mV can be observed. Keary et al., (2002), describes a causative body to straddling water table below which electrolytes in the fluids undergo oxidation and release electrons which are conducted upwards through the ore body. At the top of the ore body the released electrons cause reduction of the electrolytes; a circuit thus exists with the top of the body acting as negative terminal thus negative SP anomalies observed.

1.3.2.2 Arrays/Configurations

For this study, Wenner and Schlumberger configurations were applied. For Wenner configuration, current and potential electrodes are maintained at constant separation r, (Keary et al., 2002) all the four electrodes need to be moved between successive readings as shown in figure 6. On the other hand Schlumberger configuration has inner potential electrodes with spacing $2l$ which is smaller relative to the outer current electrodes separated by $2L$ (Figure 6). In this case several lateral movements of potential electrodes can be accommodated by a given current electrode spacing as in CST. However, for VES surveys the potential electrodes remain fixed as the current

electrodes get expanded. For measurable potentials there is the need to increase l for large L.

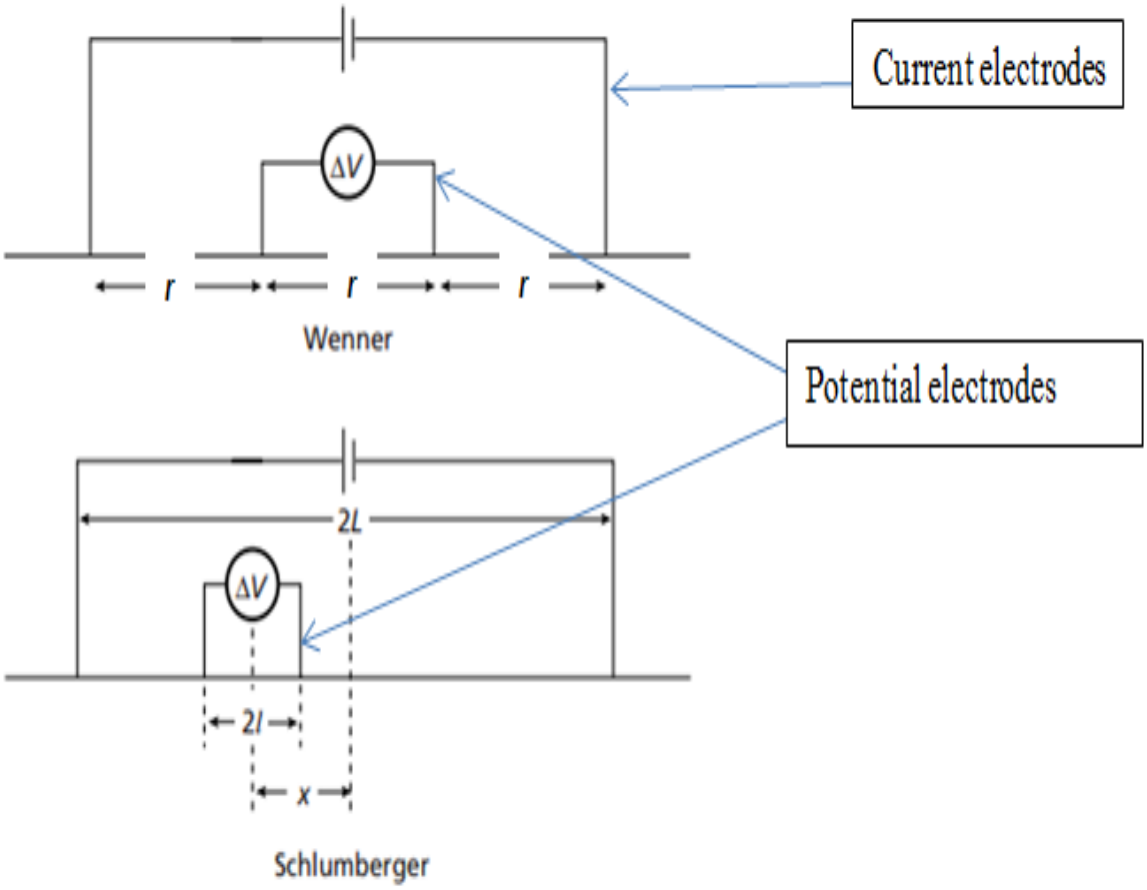

Figure 6: Wenner and Schlumberger configurations (Keary et al., 2002)

From the factors affecting resistivity of a body coupled with electrode separation in resistivity arrays, Keary et al., (2002) shows that apparent resistivity (ρ_a) for Wenner array is;

$$\rho_a = 2\pi r \frac{\Delta V}{I} \quad \text{.....} \quad 12$$

Replacing r with $\frac{L^2}{2l}$ yields equation 13, which is used in determination of apparent resistivity from Schlumberger configuration,

$$\rho_a = \frac{\pi L^2 \Delta V}{2lI} \quad \text{.....} \quad 13$$

Where; r is current electrode and nearest potential electrode separation, ρ_a is the apparent resistivity, l is the potential electrode separation, L is the current electrode separation, I is the injected current and ΔV is the potential difference.

The resistivity meter used is able to input all the variables in each of the equations 12 and 13 and out put the required value of apparent resistivity for each measurement.

1.3.2.3 Sounding Curves

Electrode configuration, layer thickness and corresponding layer resistivity are directly linked to the form of curves obtained in inversion process from sounding data over horizontally stratified medium, (Anudu et al., 2011). If three layered medium of resistivity values ρ_1, ρ_2 and ρ_3 is considered, the relative values of resistivity would define the type/form of curve obtained, each giving specific geotechnical inference as far as subsurface mapping is concerned, (Keary et al., 2002). Interpretation of apparent resistivity curve first entails realization of the curve shape then evaluated from the four basic curve types or a combination for complex situations; letters are used to refer to the

curves for convenience as shown in figure 7. Type H, for example shows that a relatively low resistivity layer (ρ_2) is bounded by a resistive overburden (ρ_1) and a high resistant basement (ρ_3), ordered as $\rho_1 > \rho_2 < \rho_3$.

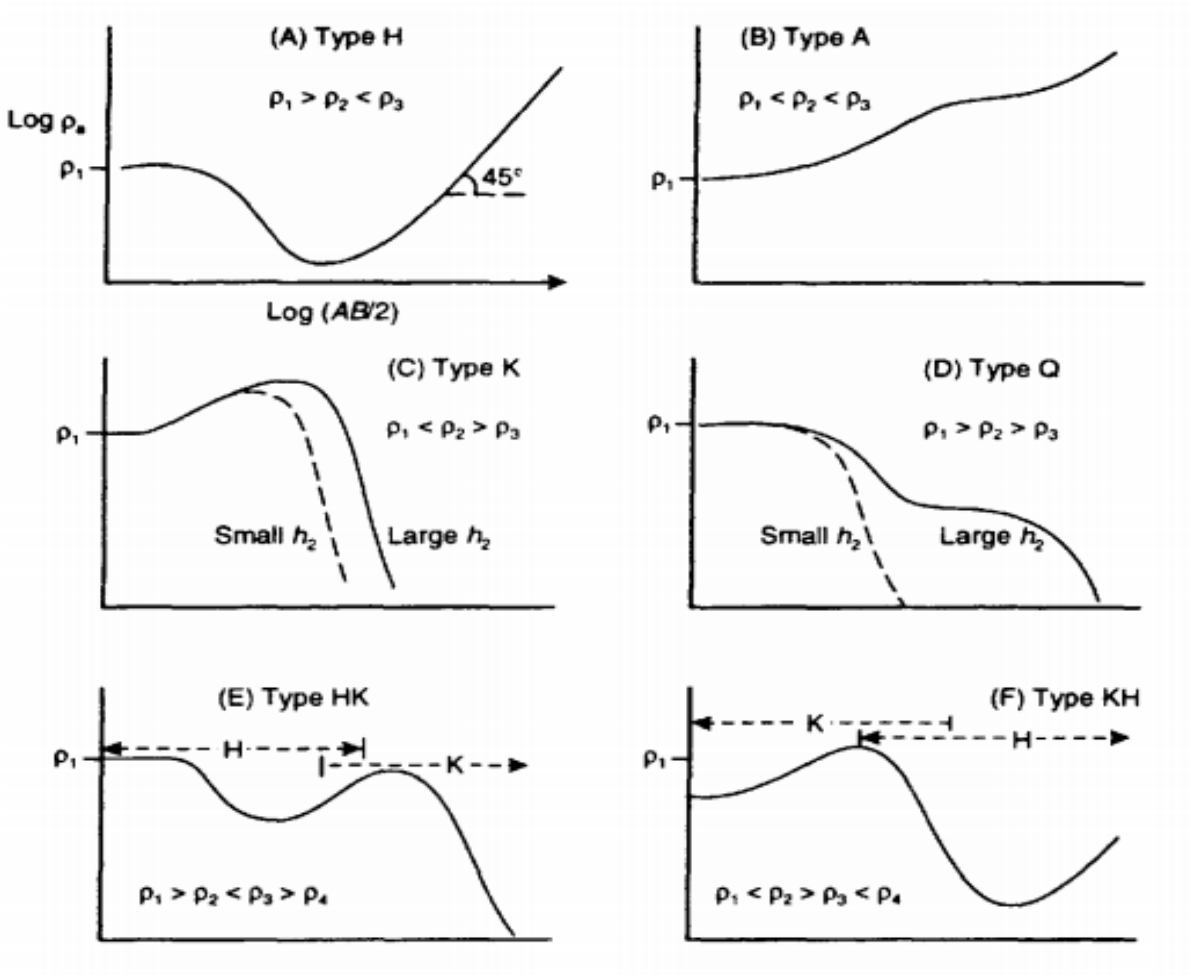

Figure 7: Resistivity sounding curves, (Reynolds, 1998)

1.3.2.4 Dar Zarrouk Parameters

This is a common reference to characteristic parameters for a geo-electric unit originating from layer resistivity (ρ) and corresponding layer thickness (h). For n -

layered unit the parameters shown in table 1 can be obtained using results from resistivity measurement i.e. product of aquifer thickness and its resistivity value gives transverse resistance (Reynolds, 1998).

Table 1: Geo-electric parameters, relationships and units

Parameter	**Definition**	**Unit**
Longitudinal Conductance	$S_L = \frac{h}{\rho}$	mS
Transverse Resistance	$R = h * \rho$	Ωm^2
Longitudinal Resistivity	$\rho_L = \frac{h}{S}$	Ωm
Transverse Resistivity	$\rho_T = \frac{R}{h}$	Ωm
Anisotropy	$A = \frac{\rho_T}{\rho_L}$	

Among the parameters, Total transverse resistance (R) has direct relation with transmissivity (T) where higher values are associated with groundwater potential zones (Anudu et al., 2011). Moreover, the zones of high transmissivity normally depict high values of total longitudinal conductance (S). Surface resistivity method, as suggested by Utom et al., (2012), can provide useful method of obtaining information on aquifer properties such as transmissivity and hydraulic conductivity in situations where pumping test data are sparse or totally lacking. For hard rock systems estimation of aquifer parameters has recorded successes by application of geophysical methods since pumping

tests assumes flow through porous medium with simple flow geometry which is not a true reflection of complex nature of crystalline rock systems and thus a modification of the models that apply to the hard rock systems has been suggested (K'Orowe, Nyadawa, Singh, and Ratnakar, 2011).

A hydro-resistivity map of these parameters gives a good platform for locating best sits for boreholes (Anudu et al., 2011). Application of Transverse resistance has been equally useful in correcting effects of difficulties encountered in VES curves interpretation such as heterogeneity effect among others (Harb, Haddad, & Farkh, 2010). This aspect was echoed by Lateef, (2012), that highest transverse resistance values corresponds to zones with highest borehole yields.

Generally aquifer transmissivity can be determined using hydraulic conductivity(K) and aquifer thickness (h) as defined by equation 14 (Utom et al., 2012).

$$T = Kh \quad \ldots\ldots\ldots\ldots\ldots\ldots\ldots\ldots\ldots\ldots\ldots\ldots 14$$

The value of hydraulic conductivity can be estimated by comparing various relations between it and aquifer resistivity, or direct relationship between transmissivity and aquifer bulk resistivity developed in fields of similar nature in the absence of field hydrological measurements such as pumping tests.

Jiri, (1993) tabulates ranges of calculated transmissivity values for aquifers in terms of transmissivity magnitude, classification, designation and supply potential. The magnitudes are measured as m^2/day (Table 2). The table shows that transmissivity

values above 100 m^2/day is an indication of good yield aquifers with wider areas of groundwater supply.

Table 2: Transmissivity Classes

Transmissivity magnitude	Class	Designation	Groundwater Supply potential
$T > 1000$	I	Very High	Withdrawals of great regional importance
$100 < T \leq 1000$	II	High	Withdrawals of lesser regional importance
$10 < T \leq 100$	III	Intermediate	Withdrawals for local water supply
$1 < T \leq 10$	IV	Low	Smaller withdrawals for local water supply
$0.1 < T \leq 1$	V	Very low	Withdrawals for local supply with limited consumption
$T \leq 0.1$	VI	Imperceptible	Sources for local water supply is difficult

1.3.2.5 IPI2 Win

This is computer software for analyzing geo-electrical data from one or more VES points obtained from various electrode configurations. The general procedure includes data input, data error correction, addition of data points and cross-section creation, (Kurniawan, 2009). The required input data includes current electrode separation, potential difference, injected current and geo-electric factor values or indirectly inputting current electrode separation and apparent resistivity values.

The software uses curve matching technique to process the input data and by inversion, geo-electrical sections with their corresponding layer thicknesses, depth and resistivity values are obtained. This information is useful in determination of geo-electric parameters that characterizes the subsurface layers under investigation.

1.3.2.6 EULER Software

Euler 1.0 is two dimensional computer software used to image subsurface depth magnetic and gravity sources using potential field derivatives, (Cooper, 2001). With profile data, inclination, declination, flight height, structural index and background normal total magnetic field as input in magnetic data analysis, Euler 1.0 can generate horizontal and vertical gradient curves as well as source location of possible geological structures by least square method using the equation 10 and 11 given in section 1.3.1.2 and section 1.3.1.3.

1.3.2.7 SURFER Software

Surfer is a grid-based mapping program useful in qualitative analysis. The software has evolved into a number of versions over time; Surfer 10 version was applied in this research. The software interpolates irregular spaced data into regularly spaced data thus allowing development of representative maps that best suits desired outcome. Data input can be done directly into worksheets with specified columns or by simple importation. In this study Surfer 10 was mainly used to develop contour maps, map digitization and

to generate cross-section data for further quantitative analysis. Kriging was the gridding method used since it best reveals trends in data distribution, (Cooper, 2001).

1.4 Statement of the Problem

The study area (Matuu-Kilango) and Machakos at large have few boreholes used to access groundwater as an alternative to scarce surface water. Ndeto, (2011) reporting on water projects in the district within which this study was conducted asserted that more than 20% of the boreholes in Yatta district have failed. This he attributed to either by unsuccessful drilling or drying up after short period of usage. The sinking of the existing boreholes in the area mainly depended on geological reconnaissance report, others done without pre-drilling survey needed. This has proved insufficient based on the high rate of failure. The completed integrated geophysical survey of the area has contributed towards an attempt to eliminate/reduce this failure rate by giving reliable information on best locations to site these boreholes by incorporating more than one technique.

1.5 Objectives

1.5.1 General objective

To carry out integrated geophysical survey involving magnetic and resistivity measurements for groundwater potential evaluation in Matuu-Kilango area

1.5.2 Specific Objectives

1. To identify ground water primers.
2. To establish aquifer geometry.
3. To develop conceptual model of groundwater potential for the survey region.

1.6 Justification

Rain water has been the main source of domestic and agricultural water in Kenya. There is therefore need to help identify alternative sources that includes underground water to fill gaps left due to rainwater scarcity. Matuu-Kilango area in Yatta is one of the worst hit areas in Kenya by water scarcity. This area is underlain by hard rocks in which aquifer formation originates from secondary porosity through fractures/faults development and a single surface technique cannot sufficiently identify these zones. Suggestions emanating from this research, of approximate aquifer geometry; extents, thicknesses and depths, will be useful for proper drilling plan.

CHAPTER TWO

MATERIALS AND METHODS

2.1 Introduction

This chapter involves the description of instrumentation, data collection procedure and processes involved in data analysis for magnetic and resistivity techniques applied in this research. Since evaluation of groundwater potential in the study is the main focus, the procedures described here were tailored to help achieve the research objectives.

2.2 Magnetic Measurements

2.2.1 Instrument

The main instrument used was a portable Geometrics G-856 Proton Precession magnetometer that measured values of total magnetic field to a resolution of 0.1 nT with an accuracy of 0.5 nT. The instrument is made up of six digit display of magnetic field value, three digit displays of station, signal strength and line number, all obtained via use of sensor bottle connected to the measuring unit. The unit uses 9 D-size industrial grade cells. The other instrument used was Trimble Juno SB type handheld GPS that was used to measure Northing, Easting and Elevation of each station or data point. Time being a critical aspect of magnetic survey, a digital watch was used.

2.2.2 Magnetic Data collection

The magnetic data collection covered 25 km^2 of the study area. Ground magnetic data was collected in the South-North direction along six straight profiles with three short

exploratory East-West oriented profiles as shown in the digitized map developed using Surfer 10 software (Figure 8). The profiles were 5 Km long each separated by a distance of one kilometer from each other. Measurements were taken at every 200 meters intervals along the South-North profiles and 100 meters for the East-West profiles, using portable Geometric 856 Proton Precession Magnetometer to a resolution of 0.1nT. A central base station was incorporated during the measurements readings taken at the station after every two hours for diurnal correction. A total of 189 measurement points were established and three readings were taken at each point to enhance accuracy. The Northing, Easting and Elevation of each station was measured using handheld GPS; Trimble Juno SB type.

Steel and other ferrous metals, power lines and other artificial magnetic sources were avoided since they are sources of magnetic noise. The magnetometer sensor was held up at approximately 4 m height then average readings recorded against time for a given station.

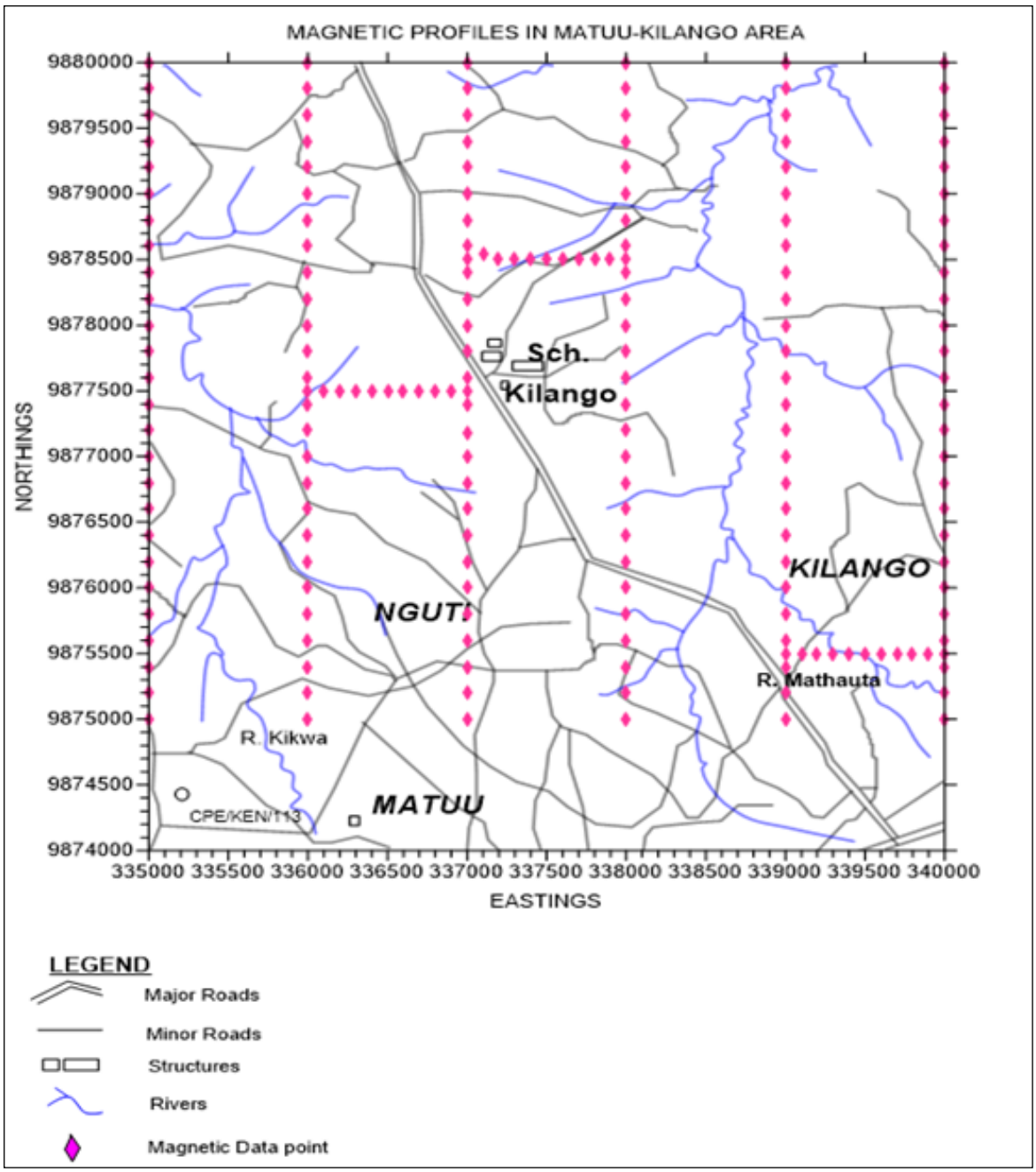

Figure 8: **Map of Matuu-Kilango area showing magnetic profiles**

2.2.3 Magnetic Data Processing and Analysis

Averages of magnetic data from the 189 stations (Appendix 1) were subjected to diurnal correction using data from base station. The effect of magnetic variation due to change in latitude (geomagnetic variation) was removed and a total magnetic intensity contour map of contour interval 50 nT was generated using surfer 10 software. From the contour plot of magnetic anomaly, cross-sections were drawn and anomaly data with linear variation defining the cross-sections were then uploaded into Euler 1.0 freeware. Taking values of Geomagnetic Intensity, Inclination, Declination and sensor height for the study area to be 33,533.8 nT, -23.0604^0, 0.4711^0 and 4 m respectively, the uploaded data was processed to obtain the corresponding Euler plots showing horizontal gradient and depth trends as well as magnetic sources.

2.3 Resistivity Measurements

2.3.1 Instrument

SARIS resistivity meter was used to obtain resistivity measurements for this survey. The equipment was able to inject electric current into the subsurface through pair of conducting electrodes and automatically compute and display apparent resistivity value for every sounding from potential difference created in the subsurface by the injected current and measured by an in-built potentiometer. Other parameters displayed include injected current value, measured potential difference, self-potential value, voltage status of the battery and standard deviation. Station coordinates were taken using handheld GPS.

2.3.2 Resistivity Data Collection

Prior to the commencement of resistivity measurements, four deep vertical electrical soundings (VES) were done adjacent to existing boreholes within and close to the study area. The resistivity values were compared with the respective borehole logging records as a control to the overall resistivity measurements. Wenner and Schlumberger arrays (Keary et al., 2002) were employed. Grids were established within which 11 measurement stations were located all within the 25 Km^2 area as shown in figure 9. Every station had its northing, easting and elevation measured using handheld Global Positioning System (GPS). Electrical resistivity measurement was done using SARIS Terrameter. Horizontal profiling by Wenner array was carried out at the established stations in the area (Figure 9) with a constant separation of 50 m. Self-potential data was captured during the Wenner array measurement; all profiles were aligned approximately parallel to the inferred river flow direction. VES by Schlumberger array method with half the spacing between current electrodes (AB/2) and potential electrode (MN/2) ranging from 1.5 m to about 200 m and 0.5 m to about 20 m respectively was then conducted within the same grids for vertical investigations. For constant monitoring of resistivity trends, logarithmic curves were drawn in situ. Forward and reversed measurements were taken to manage polarization effects.

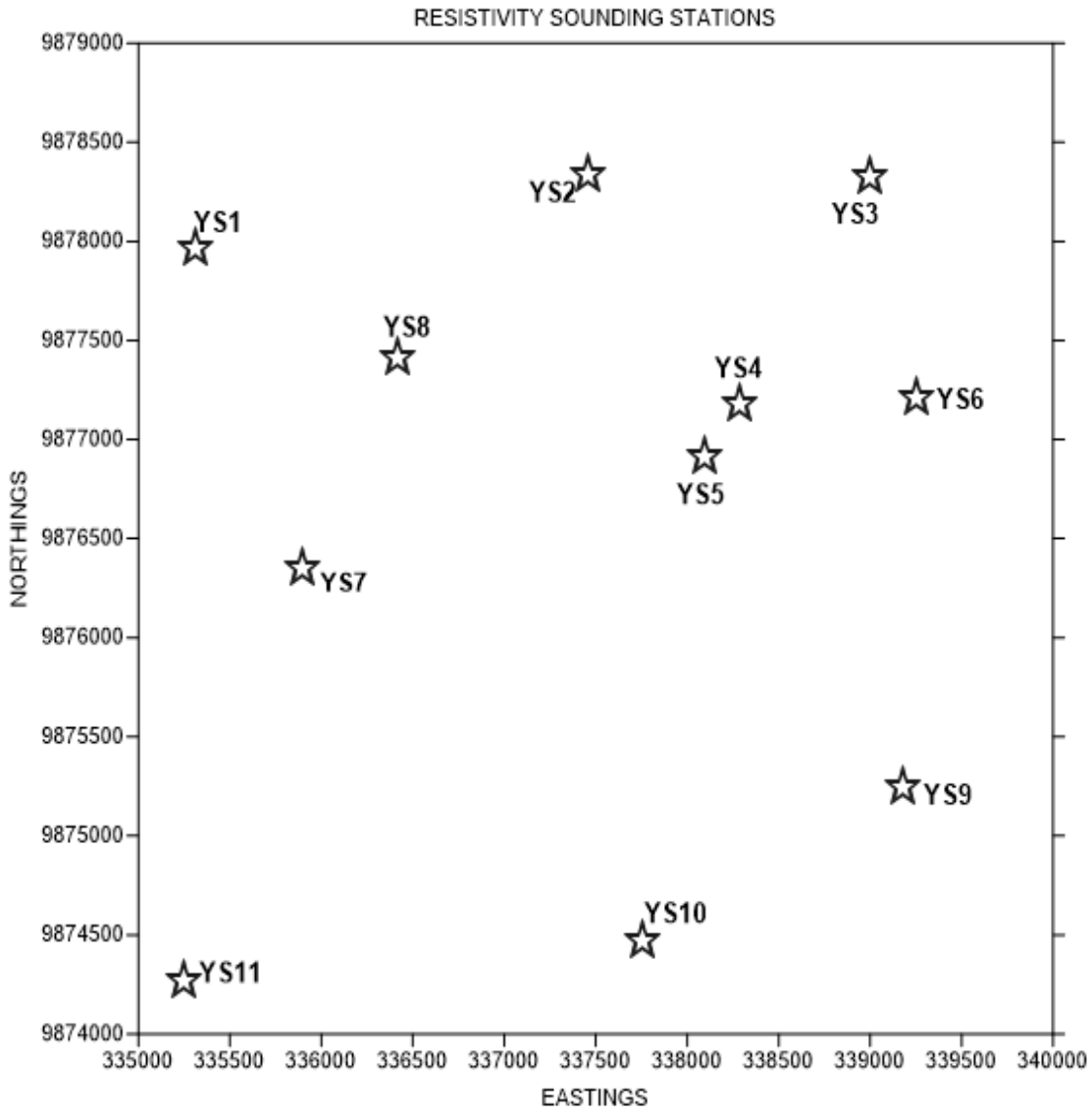

Figure 9: Resistivity Stations over the survey area

2.3.3 Resistivity Data Processing

Results from soundings carried out adjacent to existing boreholes were compared with the corresponding borehole logging information for four boreholes. Apparent resistivity data obtained from Wenner array measurements (Appendix 2) were subjected to contour

plotting using Surfer 10 software with contour interval of 10 Ωm. This was done to qualitatively map the resistivity trends across the subsurface layer lying at approximate depth of 50 m. VES data from the 11 stations, as shown in appendix 3, were subjected to digital inversion using IPI2Win software station by station and subsurface formations were mapped together with their corresponding resistivity and thicknesses. Self-potential values measured over the survey area were uploaded in Surfer 10 software and a contour map showing variation in self-potential values was generated.

In the investigation of aquifer characteristics, geo-electric parameters such as transverse resistance (R) and longitudinal conductance (S) were calculated from the inversion result using the associated equations 15 and 16 for all the vertical electrical soundings over the study area.

$$S = \sum_{i=1}^{n}\left(\frac{h_i}{\rho_i}\right) = \frac{h_1}{\rho_1} + \frac{h_2}{\rho_2} + \frac{h_3}{\rho_3} + ...\frac{h_n}{\rho_n} \quad \text{……15}$$

$$R = \sum_{i=1}^{n}\left(h_i\rho_i\right) = h_1\rho_1 + h_2\rho_2 + h_3\rho_3 + ...h_n\rho_n \quad \text{..……..…..16}$$

Where h_i , ρ_i is thickness and resistivity of the i^{th} layer of n layered geo-electrical section respectively.

This research did not include field measurements of hydraulic conductivity i.e. from pumping tests, therefore, various relationships involving hydraulic conductivities as well as transmissivity from fields of geological settings similar to that of Matuu-Kilango area

were used to estimate the transmissivity values of the identified aquifer in the study area. Calculated transmissivity values from related sites were plotted against transverse resistance values obtained for soundings that had H-Type curves and associated linear correlation coefficients obtained.

CHAPTER THREE

RESULTS AND DISCUSSIONS

3.1 Introduction

This chapter includes the presentation and discussion of research results obtained from the data processing and analysis outlined in chapter two. This is achieved with the aid of maps, figures and tables. The results and discussions include magnetic anomaly trends for qualitative inferences, 2D-Euler deconvolution for magnetic sources positioning and determination of primers such as faults and fractures quantitatively, resistivity measurement control, electrical self-potential trends, results from Wenner array data analysis, and comprehensive discussion of Vertical Electrical Sounding/Schlumberger array results as obtained from digital inversion, associated curve types and calculated geo-electric parameters. This was aimed at identification of groundwater primers and determination of inferred aquifer characteristics as far as groundwater potential evaluation in Matuu is concerned.

3.2 Magnetic Anomaly Trend

Figure 10 shows total magnetic intensity contour map of contour interval of 50 nT. The map indicates a trend in magnetic lows adjacent to magnetic high values at the western part of the study area as shown by the hachures. This can be qualitatively explained by an existing subsurface feature at the zone responsible for the anomaly. The eastern part of Matuu-Kilango area has no distinct feature as far as magnetic survey result is concerned. The southern part of the study area shows magnetic high values. This

observation is associated to the artificial structures and activities of Matuu town superimposing on the measured values.

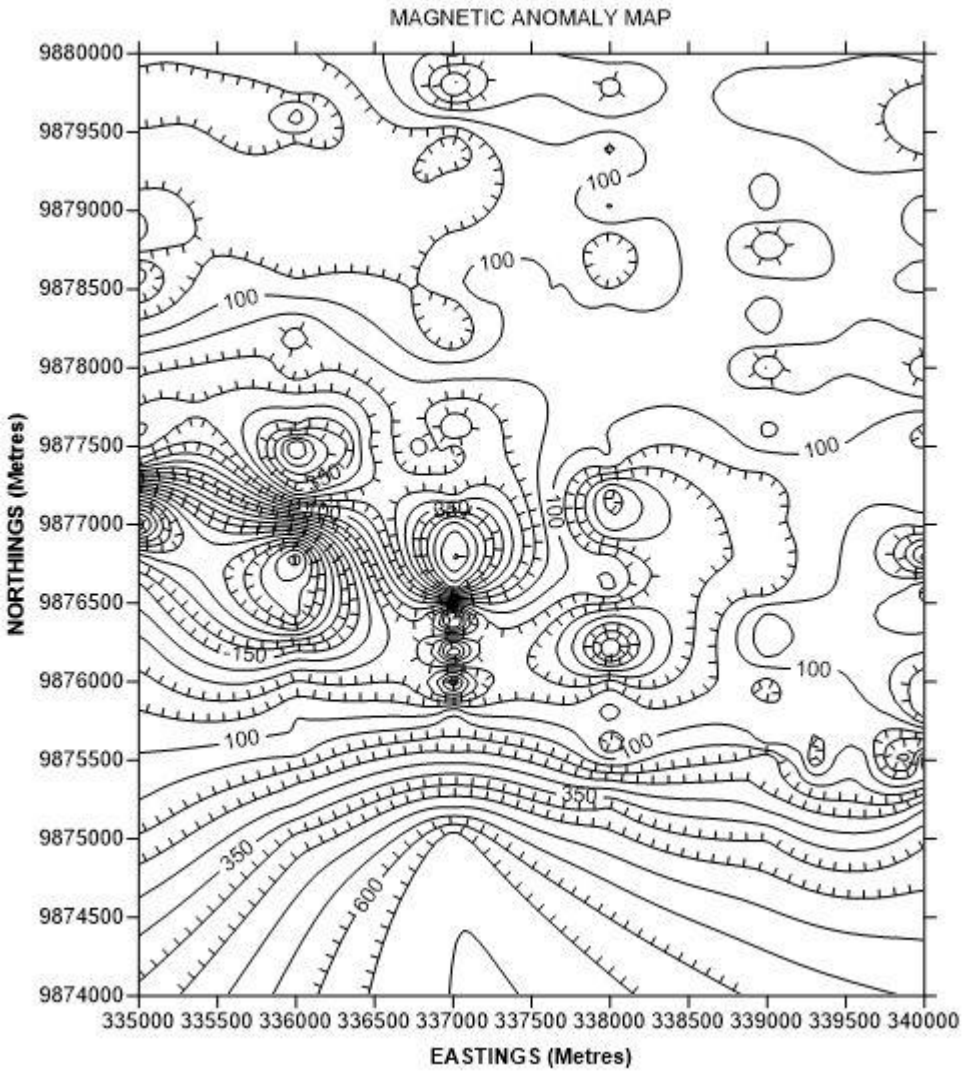

Figure 10: Magnetic Intensity contour map; hachures downhill show decreasing values of the magnetic intensity.

3.3 2D-Euler Plots

In the identification of groundwater primers, Euler plots from deconvolution allowed quantitative imaging of faults associated to groundwater. The Euler plots were generated

using data from cross-sections AA', BB', CC' and DD' over the anomalous zone of the study area (Figure 11). The dashed lines shows the cross-sections cut across the area where the magnetic anomaly was identified.

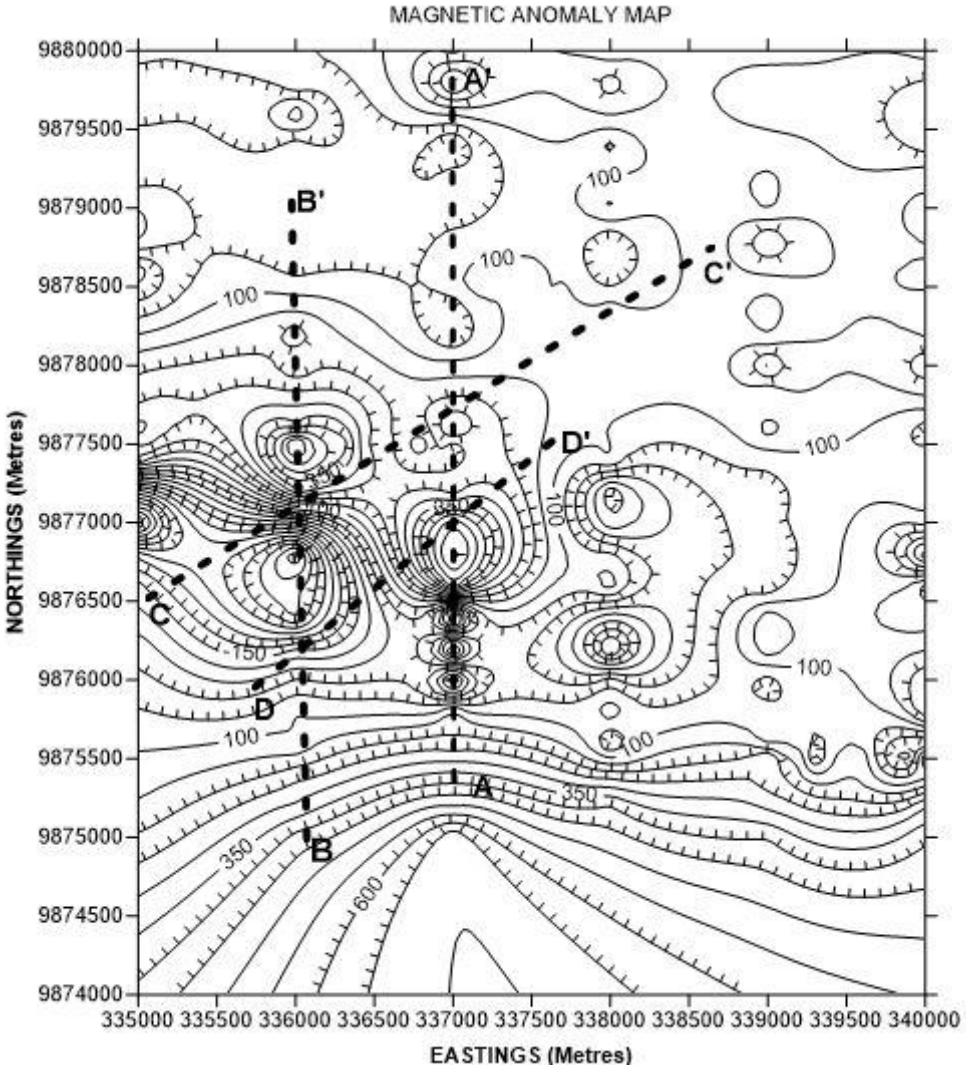

Figure 11: Cross-sections across anomalous zones

Figure 12 shows Euler solutions for cross-section AA' calculated using structural index of 0.5 which best represent faults. The horizontal and vertical gradients depict steady

increase followed by drop value of approximately 3.7 nT/m over 0.2 Km to 1.5 Km cross-section distance representing lateral variations in magnetization over the same cross-section distance range. The depth to the source depicted by best clustered solutions is shallowest (about 100 m) over the same distance range. A solution gap exist at the start of the cross-section with no clear discontinuities shown for the rest of the cross-section an indication of possible fractures but no major fault.

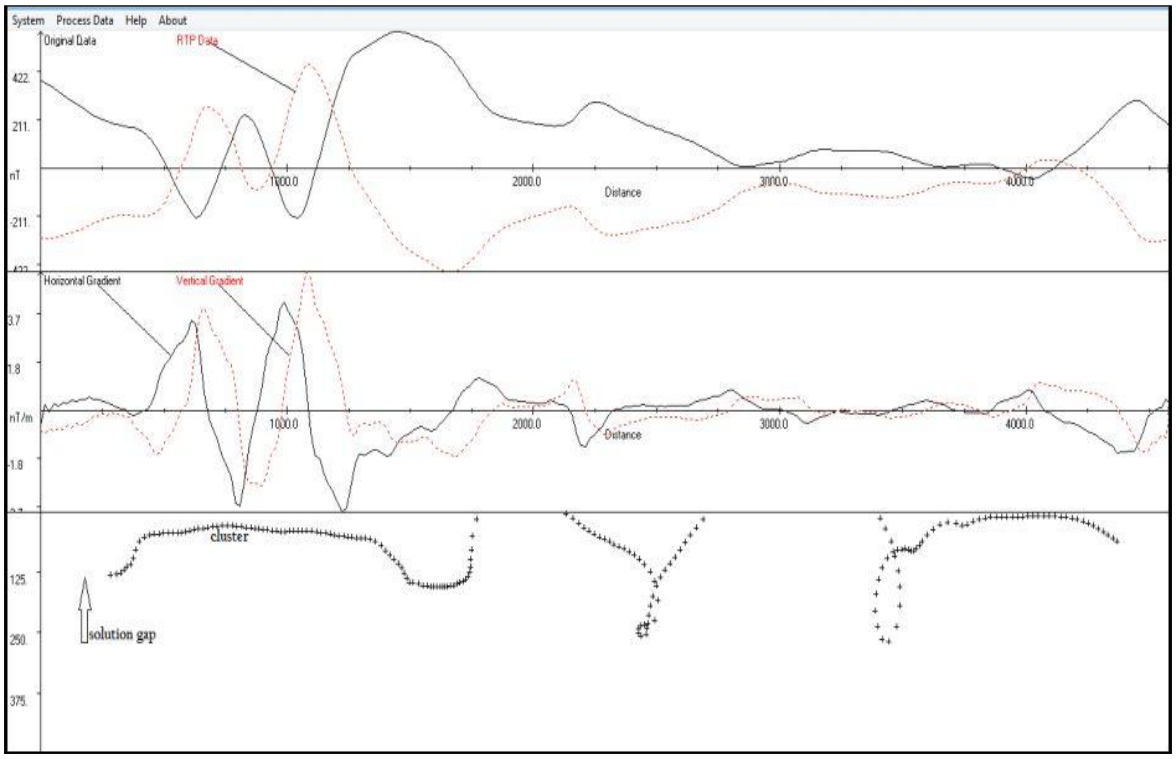

Figure 12: Euler plot for cross-section AA'

From cross-section BB', figure 13 is a result from Euler depth investigation using structural index of 0.5. For this section, the abrupt variation in horizontal and vertical gradients to a maximum value of about 3 nT/m covers a wide range of cross-section

distances, that is, from 1.2 Km to 2.75 Km along the cross-section. It is over this same region where shallowest (about 150 m), best clustered Euler solutions and a disjointed formation at about 1.5 Km cross-section length was shown, an indication of the possible fault. The deepest solution to the basement is at about 400 m from the surface.

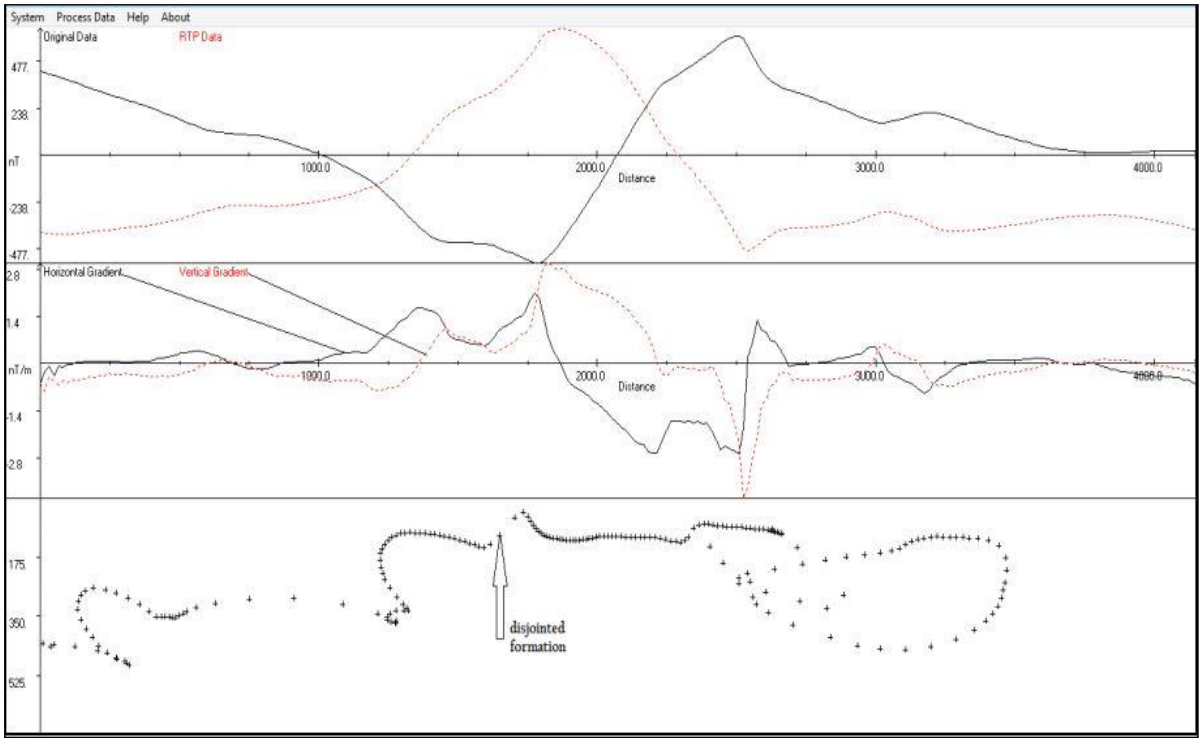

Figure 13: Euler plot for cross-section BB'

Figure 14 shows magnetic anomaly Euler solutions for cross-section CC'. A good image of subsurface structure depth was given by best cluster of solutions calculated using the most applicable structural index for fault (0.5) occurring averagely at 150 m from the surface, at cross-section distances 0.2 Km to 2.75 Km. A clear discontinuity is observed at about 1.8 Km distance along the cross-section showing an extension of the fault

inferred in BB' Euler solution analysis. Horizontal and vertical gradients vary abruptly a few meters from the start of the cross-section to a distance of 2.3 Km along the cross-section. This indicated a wide lateral variation in magnetisation. However, gradient value registered for the underlain feature is relatively small, approximately 1.2 nT/m.

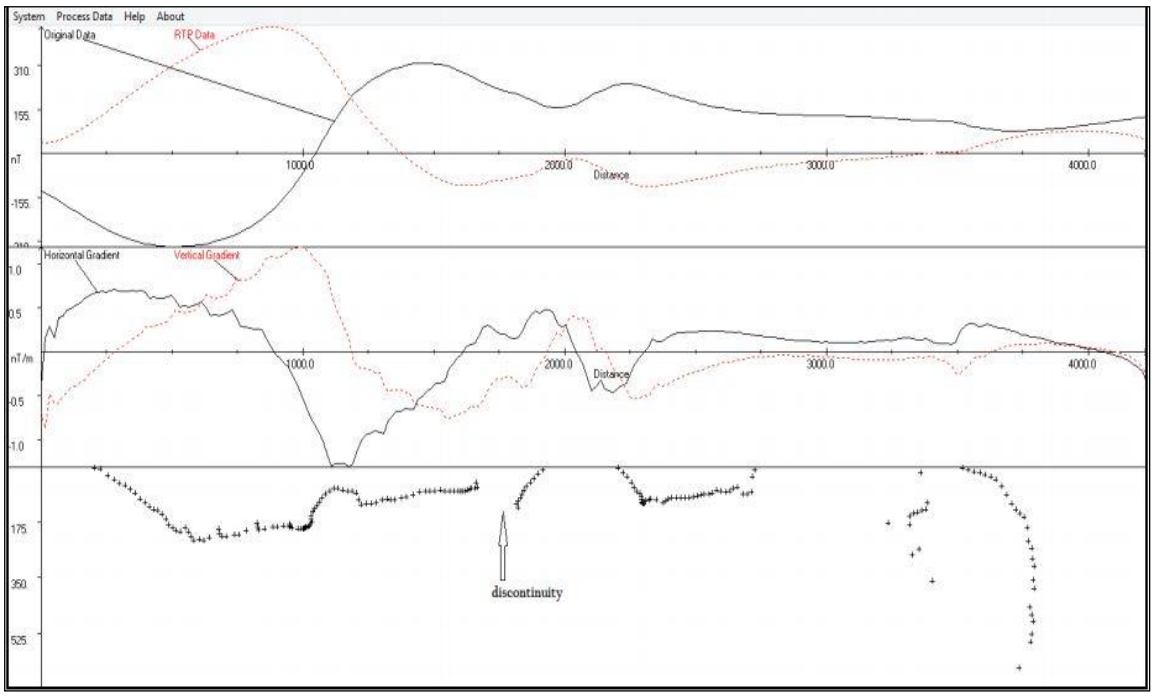

Figure 14: Euler Plot for cross-section CC'

To verify the trends in Euler solution along the possible fault inferred from Euler plots for cross-section BB' and CC', a cross-section DD' was drawn and Euler solutions determined (Figure 15). It equally showed clustered solutions with a pronounced discontinuity at about 0.9 Km profile distance. The cluster extended up to 2.4 Km cross-section distance. The result helped in the inference of the fault orientation which appeared to be in SE-NW direction.

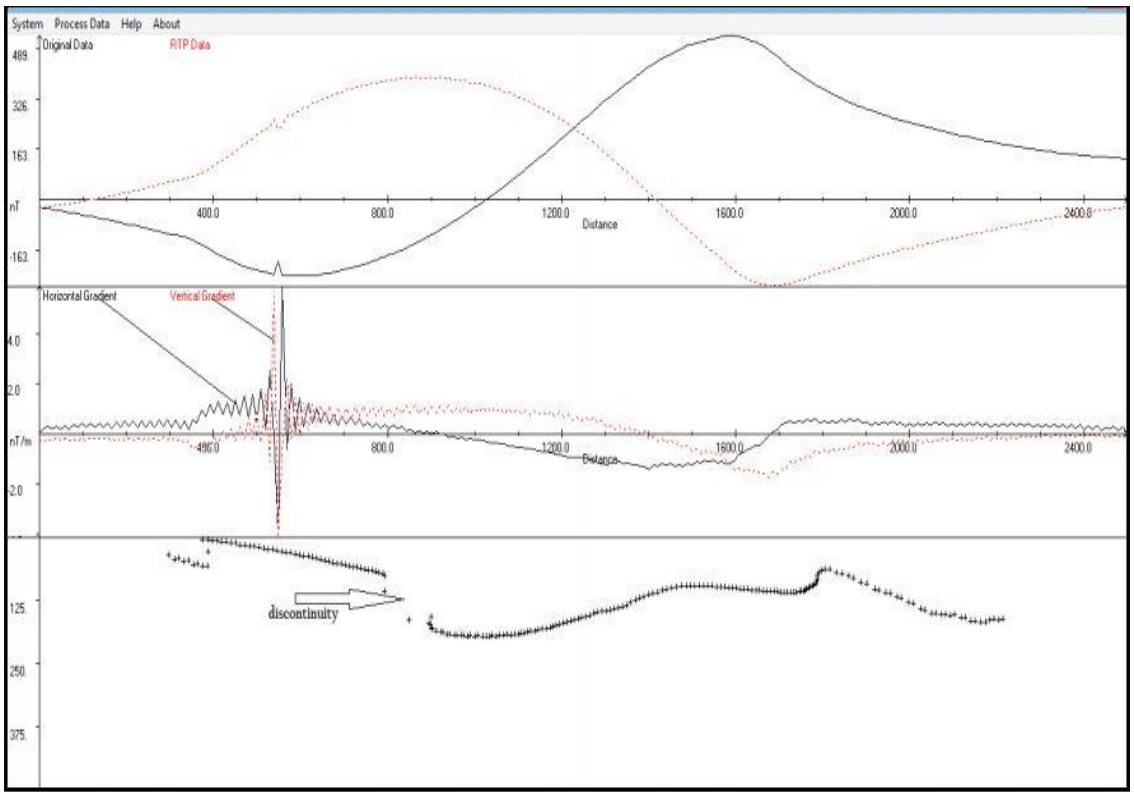

Figure 15: Euler Plot from cross-section DD'

3.4 Resistivity measurement control

Resistivity soundings carried out adjacent to already existing logged boreholes had the VES inversion result showing comparable values to the borehole logs. Figure 16 shows an example of VES carried out close to a borehole at (9873287, 0337848), the values of h in VES result is compared to the difference in the corresponding ranges in logging information i.e. a layer thickness of 1.18 metres from VES (Figure 16) is depicted on logs as 2.5 metres with the small variation associated to time difference. The comparison gave confidence in the outcome of related resistivity measurements over the study area.

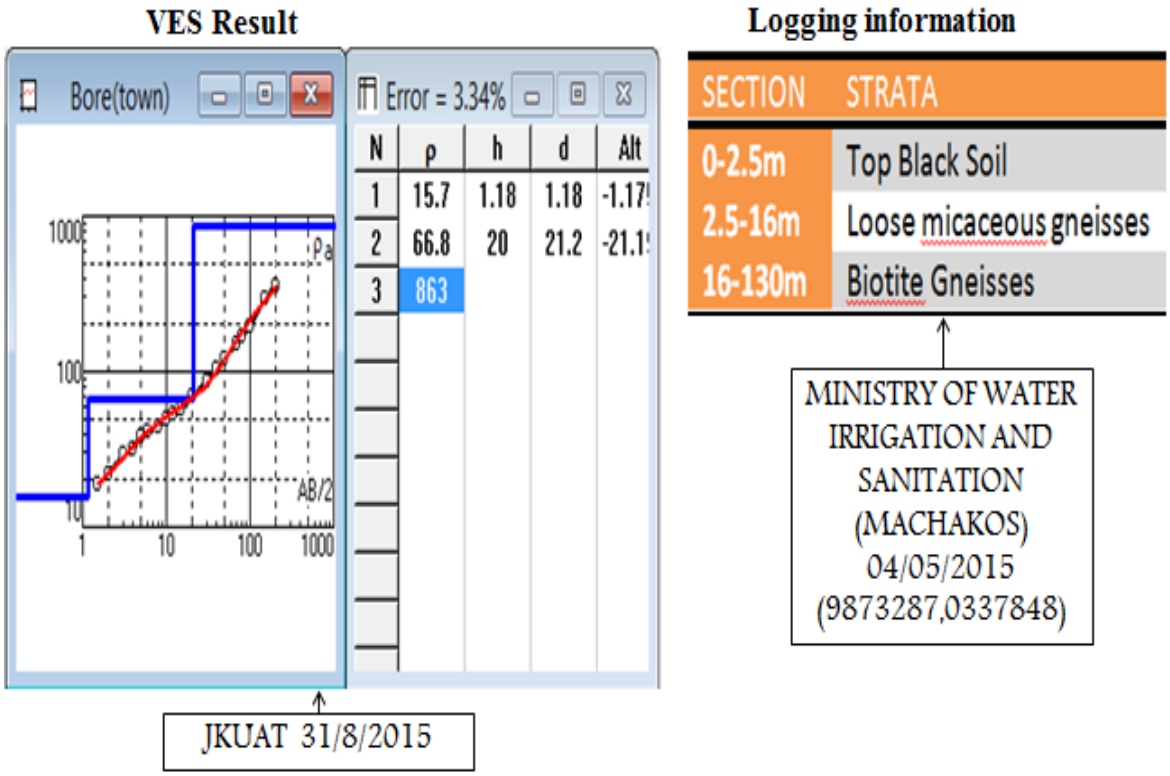

Figure 16: VES Inversion result versus borehole log report for borehole at (9873287, 0337848)

3.5 Electrical Self-Potential trends

The presence of streaming fluids or groundwater in a hard rock basement system may be associated with secondary porosity originating from faults and fractures which act as groundwater conduits. Figure 17 shows variation of SP values over the study area, one of the commonly investigated primers. The western area covered by the map depict a spread of negative SP values ranging from -10mV to about -100mV. The eastern side of the study area showed increasing positive SP values. The trend of variation in negative SP values depicts an anomaly at the west in the SE-NW direction. According to Jinadasa

and Silva, (2009); Reynolds, (1998) this car be related to weak geological structures in which groundwater accumulates. An anomalous body showing negative SP values above -100mV exist at the central zone and is associated with a conductive ore body in the subsurface.

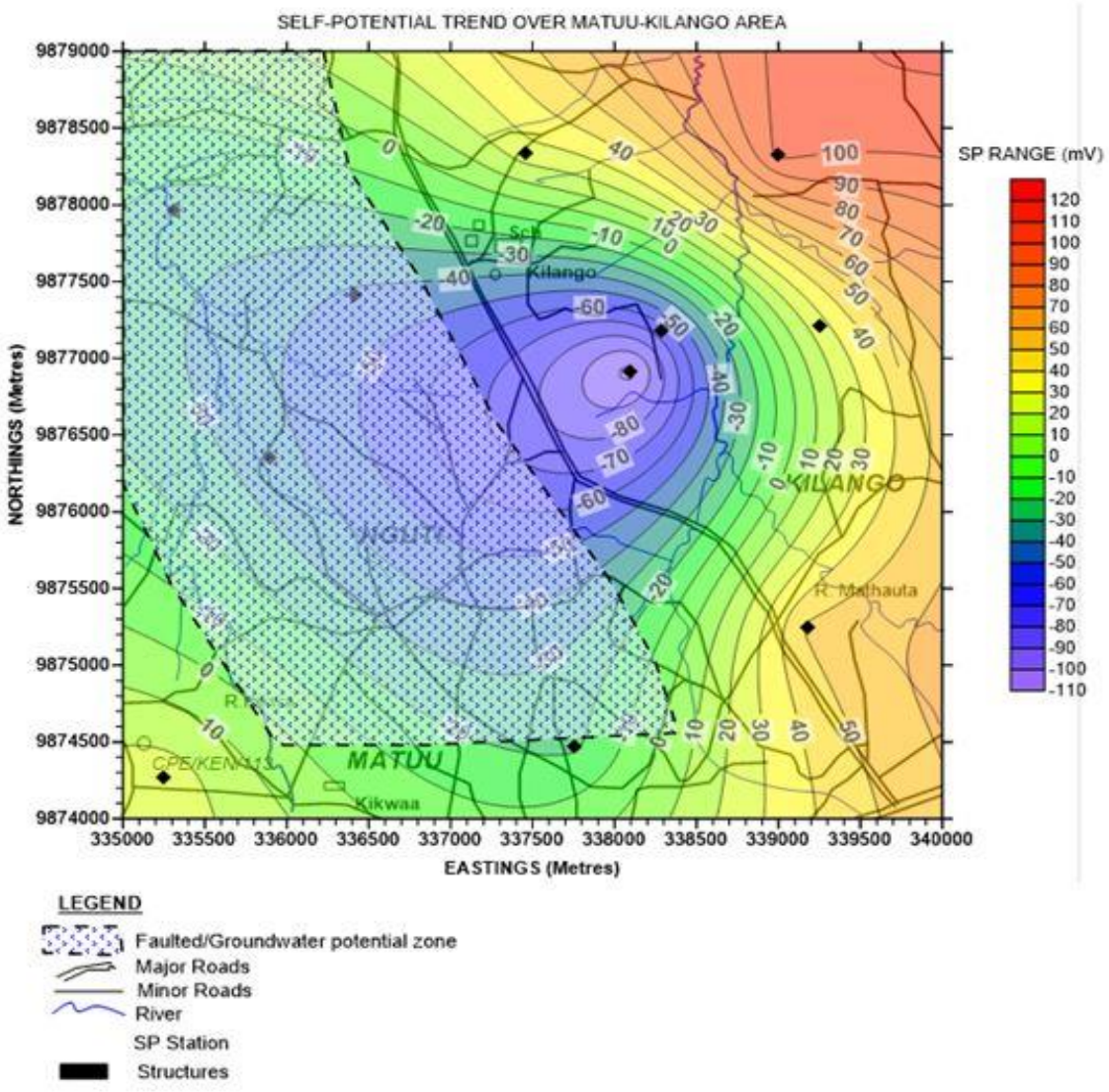

Figure 17: Self-Potential Anomaly contour map over Matuu-Kilango

3.6 Wenner Array Profiling

Wenner array measurement data (Appendix 2) was processed using Surfer 10 software and a contour map of contour interval 10 Ωm was generated (Figure 18). This gave an impression of the resistivity trend across the subsurface layer lying at approximate depth of 50 meters. An anomalous zone to the west of the study area was observed stretching from North West to South Eastern part of the study area having an average low resistivity value of 130 Ωm as shown with the red boundary in figure 18.

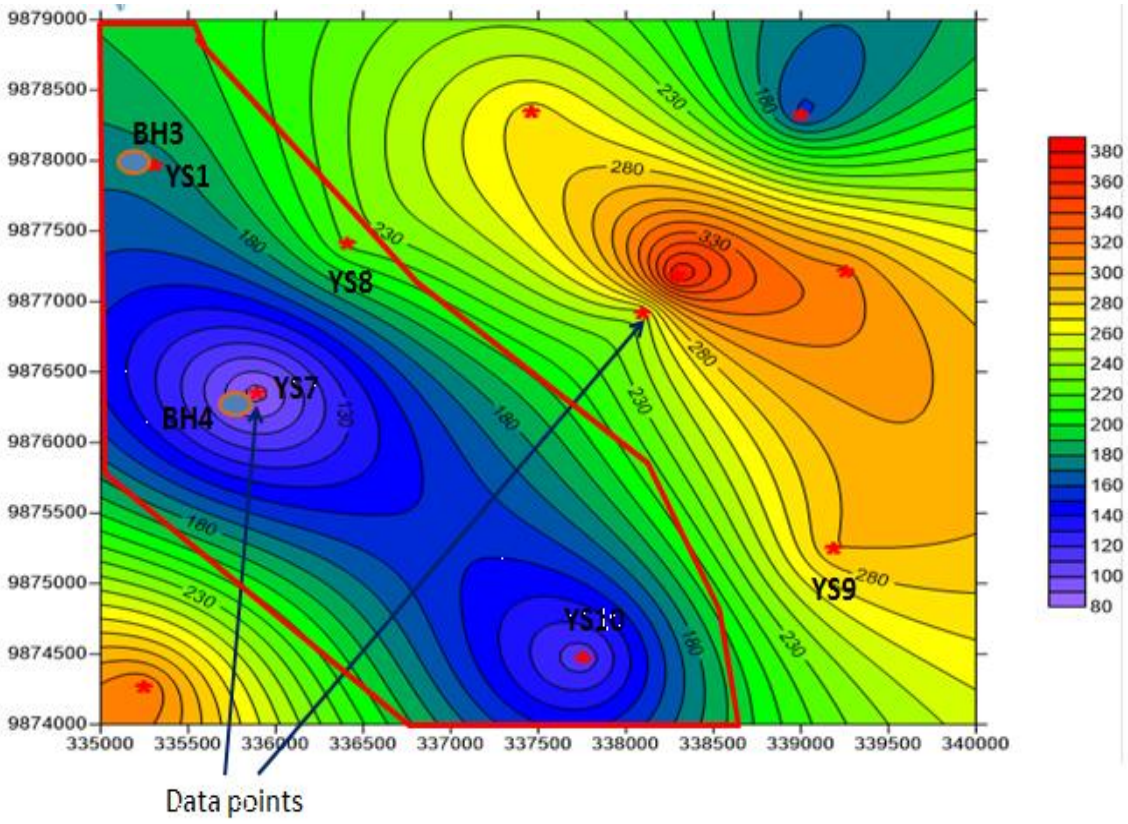

Figure 18: Contour Plot of apparent resistivity trends over the anomalous zone.

3.7 Schlumberger Array Vertical Electrical Sounding

Digital inversion involving match of curve obtained from plotting AB/2 against apparent resistivity (ρ) and a pre-installed theoretical curve yielded images of geo-electrical subsurface systems for each sounding (YS1 to YS11) giving general formation of three to four layers. Results were obtained within acceptable matching errors of less than 10%. IPI2Win window that displayed inversion results have parameters N, ρ, h, d and Alt which are number of layers, layer resistivity, layer thickness, depth at which a given layer exist and altitude respectively, the window also displays matched curves to the left and matching error as a percentage. Figure 19(a) and 19(b) shows sample inversion results of sounding conducted at the eastern and western zones of Matuu-Kilango area respectively. A low resistivity layer bounded by a high resistivity overburden and basement is groundwater primer observed from the west of Matuu-Kilango area; geologically it is referred to as an aquifer.

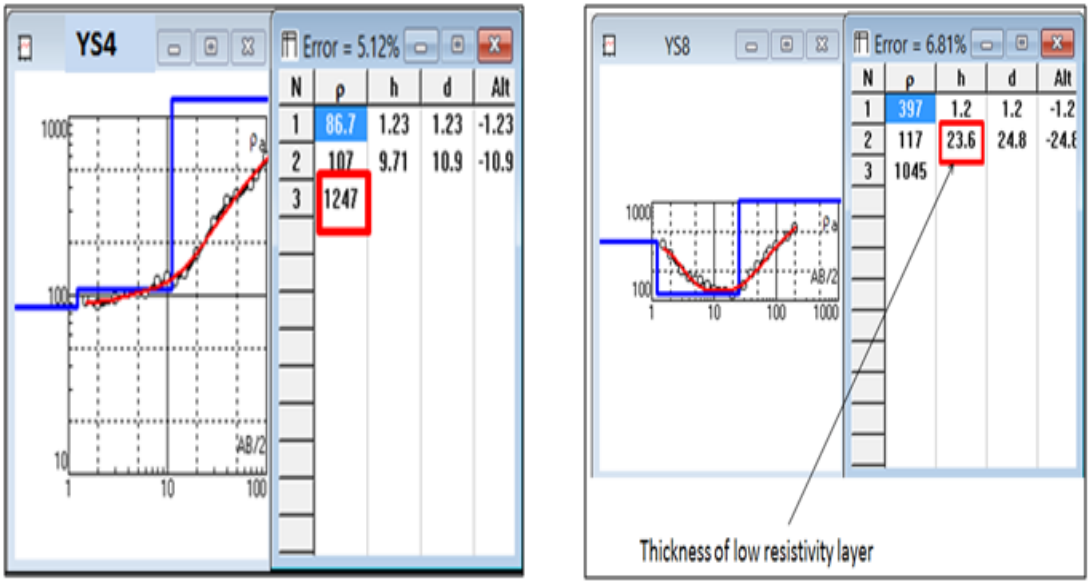

(a) *Inversion result for YS4 sounding, located at the Eastern side of the study area*

(b) *Inversion result for YS8 sounding, (west of Matuu)*

Figure 19: Sample Digital Inversion results for VES conducted over Matuu-Kilango area

Table 3 shows curve types obtained for all the 11 stations and it was evident that the soundings conducted at the western part of the study area had H curve type dominating i.e. 67% of the total H-type fall precisely at the west of Matuu-Kilango area. This is an indication of an inferred aquifer (Anudu et al., 2011), defined by low resistivity layer bounded by an overburden and resistive basement. The curve types associated with the eastern zone, majorly the A-type, depict subsurface with increasing resistivity with depth. This is in agreement with what was observed at the field as area dominated with hard rock outcrops.

Table 3: Table showing Curve types associated to VES inversion results

VES Station Code	Curve Type analysis	
	Curve nature	**Type**
YS1	$\rho_1 > \rho_2 < \rho_3$	H
YS2	$\rho_1 > \rho_2 < \rho_3$	H
YS3	$\rho_1 < \rho_2 < \rho_3 < \rho_4$	AA
YS4	$\rho_1 < \rho_2 < \rho_3$	A
YS5	$\rho_1 > \rho_2 < \rho_3$	H
YS6	$\rho_1 > \rho_2 < \rho_3$	H
YS7	$\rho_1 > \rho_2 < \rho_3$	H
YS8	$\rho_1 > \rho_2 < \rho_3$	H
YS9	$\rho_1 < \rho_2 > \rho_3 < \rho_4$	KH
YS10	$\rho_1 < \rho_2 < \rho_3$	A
YS11	$\rho_1 < \rho_2 < \rho_3$	A

In the investigation of aquifer characteristics as well as geo-electric parameters, transverse resistance (R) and longitudinal conductance (S) calculated from the inversion

result for all the vertical electrical soundings over the study area showed relatively high values dominating the western zone soundings (Table 4).This can be attributed to the potential for groundwater being greater at the western part of the study area than it is to the East. Notable trends in the calculated R and S as well as relative thicknesses of the delineated low resistivity layer existed with the western VES results i.e. the values were found to increase towards the North as evident from YS9, YS7, YS8 and YS1 sounding results, this shows an increasing borehole yield northwards.

Table 4: Table of calculated geo-electrical parameters for aquifer characteristic evaluation

VES Station Code	Parameters	
	Transverse Resistance (Ωm^2)	**Longitudinal Conductance (mS)**
YS1	11523.12	0.306062
YS2	3275.93	0.088506
YS3	23908.67	0.555043
YS4	1145.611	0.104935
YS5	4023.946	0.097382
YS6	2867.9	0.150078
YS7	880.02	0.434947
YS8	3224.7	0.203885
YS9	2935.598	0.071684
YS10	653.5612	0.586065
YS11	4405.328	0.225382

3.8 Transmissivity Attributes

Determination of transmissivity attributes of the aquiferous zones of Matuu is among the key aspects in evaluation of groundwater potential of the area. To establish this, eight regions of hard rock formations namely Oban Massif in Nigeria, Goa in India, Kabatini Well Field of Kenyan Rift, Ondo State of Southwestern Nigeria, Sinai fields of Egypt, Kaduna in Nigeria, Central Finland, and Godavari-Purna, were considered in estimating the transmissivity values for Matuu. Three theoretical, four experimental and one empirical relations between transmissivity and related parameters from the considered areas were used with the resistivity results of this survey to arrive at transmissivity estimates discussed in this section.

T_1 displays values of transmissivity obtained using theoretical relationship between aquifer bulk resistivity and hydraulic conductivity, (equation 17), applied for Oban Massif area whose geological setting is 75% covered by Gneiss and its fractures closed with open ones filled with quartz, biotites and chlorites (Edet & Okereke, 2015).

$$\rho = 1680 * K^{-0.87} \quad \ldots\ldots\ldots\ldots\ldots\ldots \quad 17$$

The product of K from equation 17 and aquifer thickness (h) gives the expression of T_1;

$$T_1 = h\left(\sqrt[0.87]{\frac{1680}{\rho}}\right) \quad \ldots\ldots\ldots\ldots\ldots\ldots \quad 18$$

The relationship (Equation 17) was used to calculate hydraulic conductivity values, which together with respective aquifer thicknesses was used to determine the transmissivity values (T_1). The transmissivity values (T_1) are far much above 100 m^2/day

indicating high yields. Figure 20 shows a correlation plot of transmissivity (T_1) against transverse resistance values (R) obtained from resistivity measurements of Matuu-Kilango groundwater potential zone. A correlation coefficient of 0.6004 was obtained.

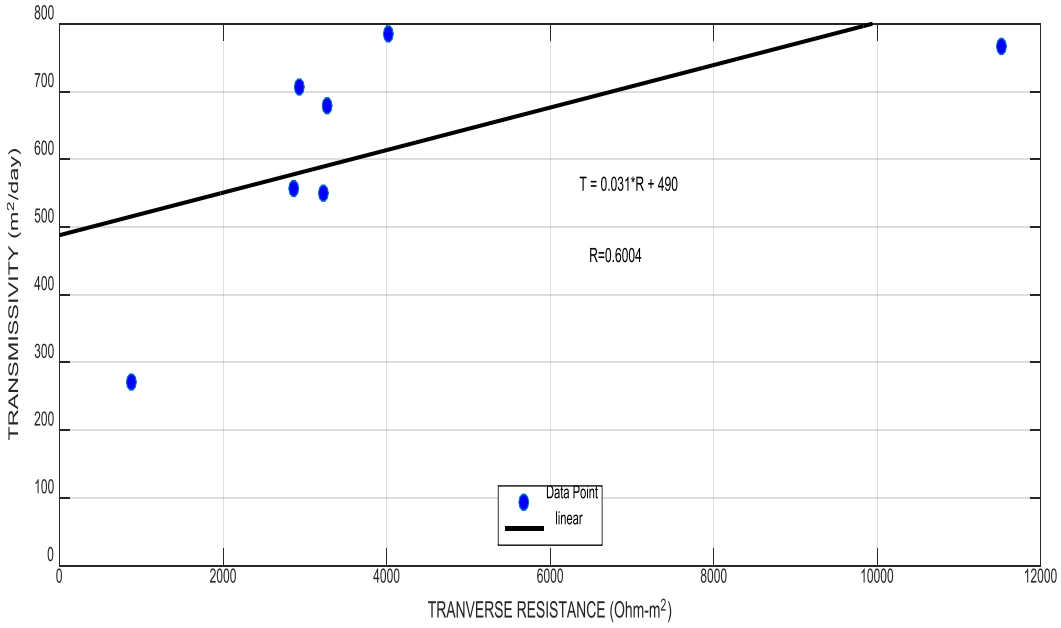

Figure 20: Plot of Transmissivity against Transverse resistance relative to geological origin of Oban Massif field, Nigeria.

The calculated transmissivity values (T_2) shown in table 5 were determined from an experimental relationship between transverse resistance and transmissivity indicated by equation 19. The equation shows linear relationship between the investigated parameters, developed for West Coast Laterites of Goa in India whose geological setting is described by quartz, chlorite, biotites Schist capped with variable thickness of laterites generally hard rock system (Chachadi & Gawas, 2012). The values obtained for

transmissivity plotted against corresponding transverse resistance values for soundings that generated H-Type curves from resistivity analysis (figure 21), displayed strong correlation coefficient of 0.9971. All the calculated transmissivity values were above 100 m^2/day limit except sounding YS7.

$$T_2 = 0.59R - 58.7296 \quad \ldots\ldots 19$$

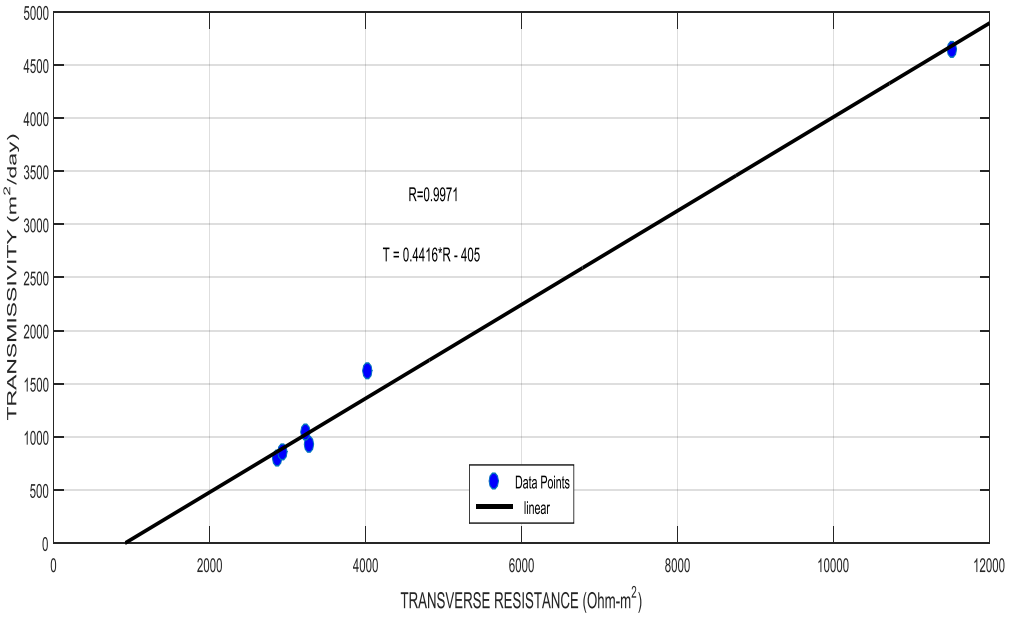

Figure 21: Plot of Transmissivity against Transverse resistance relative to geological formation of Goa field, India.

Equation 20 shows an experimental power relationship between transmissivity and bulk resistivity developed for Kabatini Well Field, Upper Lake Nakuru Basin within the Kenya Rift Valley geologically defined by Basalt rocks composed of mafic minerals and sub-ordinate quartz (Sosi, Cheboi, & Simiyu, 2013). Substituting the aquifer resistivity

values, the equation was used to calculate the transmissivity values (T_3) shown in table 5 and then plotted against transverse resistance values of the corresponding soundings (Figure 22).

$$T = 1.429 \times \rho^{0.585} \quad \text{..... 20}$$

A linear relationship between transmissivity (m^2/day) and transverse resistance (Ohm-m^2) was achieved (Equation 21) with a correlation coefficient of 0.5725. The calculated values of transmissivity were found to fall in class II (Table 2) thus high yields of regional importance.

$$T = 0.0309R + 470 \quad \text{.....21}$$

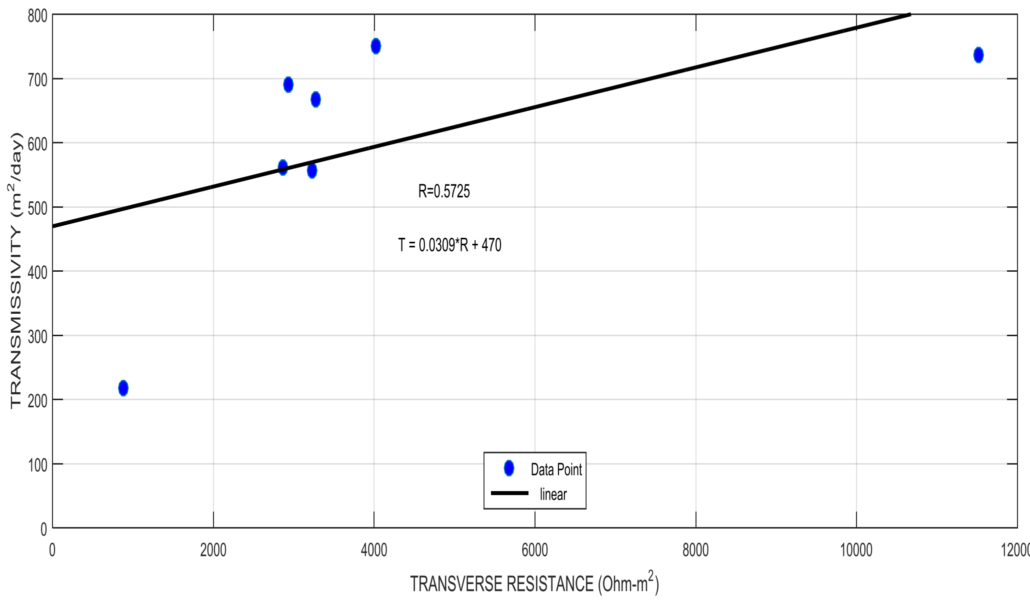

Figure 22: Plot of Transmissivity against Transverse resistance relative to geological formation of Kabatini Well Field, Kenya Rift Valley.

From basement complex areas of Ondo State, Southwestern Nigeria a theoretical relationship between hydraulic conductivity and aquifer bulk resistivity shown by equation 22 was developed for fractured and faulted basement rocks made of granite gneiss, biotites gneiss, quartzite and Charnokite (Mogaji et al., 2011). Equation 22 was useful in estimation of hydraulic conductivity values which were used together with aquifer thicknesses to generate transmissivity values (T_4) shown in table 5.

$$K = 0.0538 \times e^{0.0072\rho} \quad \ldots\ldots\ldots\ldots\ldots\ldots\ldots\ldots\ldots\ldots\ldots\ldots\ldots\ldots\ldots\ldots\ldots\ldots\ldots\ldots\ldots\ldots\ldots\ldots 22$$

From the product of equation 22 and aquifer thicknesses (h), the expression used to generate transmissivity values (T_4) shown by equation 23 was obtained;

$$T_4 = 0.0538he^{0.0072\rho} \ldots\ldots\ldots\ldots\ldots\ldots\ldots\ldots\ldots\ldots\ldots\ldots\ldots\ldots\ldots\ldots\ldots\ldots\ldots 23$$

The plot in figure 23 shows comparison of transmissivity with calculated transverse resistance for Matuu-Kilango groundwater potential zone. A linear correlation (Equation 24) with a correlation coefficient of 0.9957 was realized. This linearity observed describes the property of an aquifer with good subsurface water flow.

$$T = 0.001086R - 0.7141 \ldots\ldots\ldots\ldots\ldots\ldots\ldots\ldots\ldots\ldots\ldots\ldots\ldots\ldots\ldots\ldots 24$$

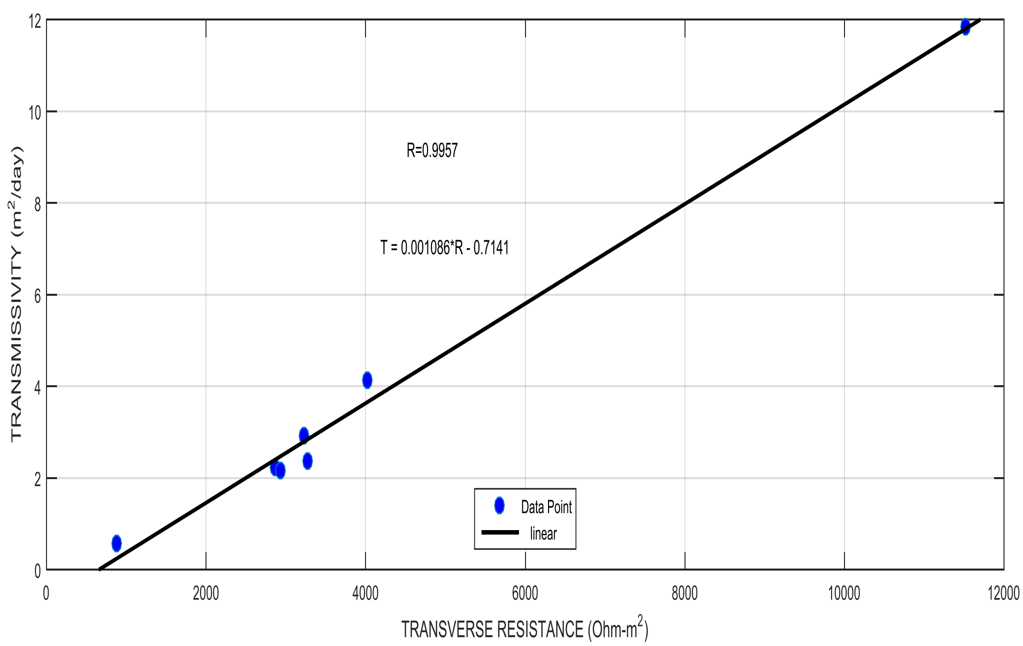

Figure 23: Plot of Transmissivity against Transverse resistance relative to geological formation of Ondo State, Southwestern Nigeria.

A quadratic relationship between hydraulic conductivity and aquifer resistivity shown by equation 25 was developed from experimental results of groundwater survey in from

central Sinai fields in Egypt, with Cretaceous Sandstones forming its basement, (Usama, Fernando, Mohamed, Ayman, and Abbas, 2010). The estimated hydraulic conductivity values together with corresponding aquifer thicknesses were useful in calculation of transmissivity values (T_5) for aquifers in Matuu (Table 5). The transmissivity values obtained were relatively high i.e. many falling in class I with only one in class II, as far as aquifer classification is concerned (Table 2).

$$K = 0.012\rho^2 - 1.2\rho + 35 \quad \ldots\ldots 25$$

A plot of transmissivity against transverse resistance (figure 24) from which we note a linear relationship (equation 26) with a correlation coefficient of 0.9817 was obtained showing a strong correlation between the parameters. This equally explains flow capability of the aquifer under investigation.

$$T = 1.312R - 1818 \quad \ldots\ldots 26$$

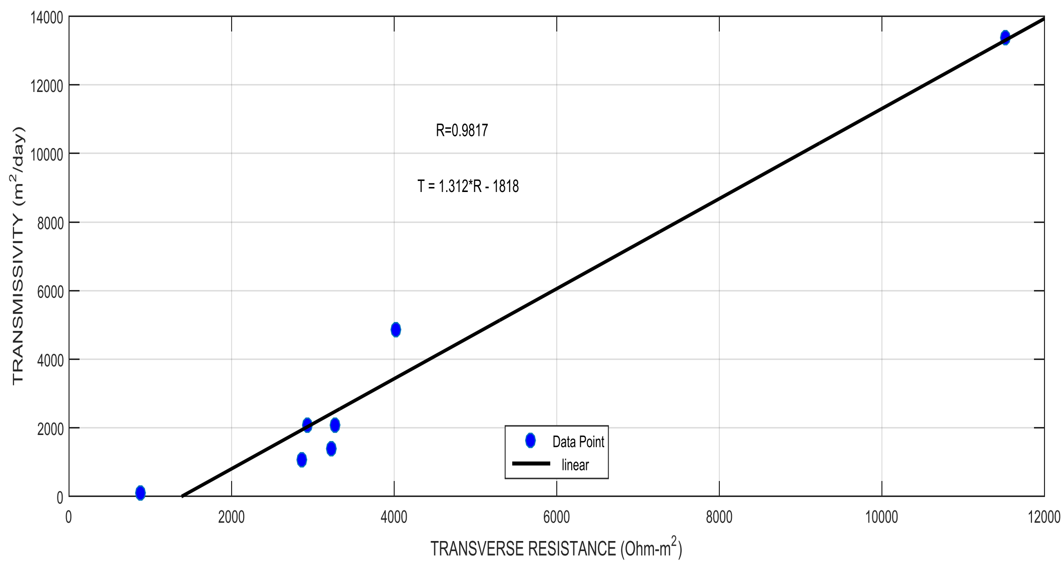

Figure 24: Plot of Transmissivity against Transverse resistance relative to geological formation of Central Sinai, Egypt.

Figure 25 is a plot of estimated transmissivity values of Matuu groundwater potential zone against transverse resistance values calculated over the same area. The transmissivity values were obtained using equation 27 developed from a theoretical relation between hydraulic conductivity, aquifer thickness and bulk resistivity (equation 28) generated from weathered crystalline basement rocks of Kaduna in Nigeria underlain by magmatite-gneiss complex and Schist with thick overburden overlying fractured zones (Kudumnya & Osumeje, 2015). 71% of the calculated transmissivity values were found to be above 100 m^2/day high yield limit.

$$K = 8\times10^{-6} he^{-(0.0013\rho)} \quad \ldots\ldots\ldots\ldots\ldots\ldots\ldots\ldots\ldots\ldots\ldots\ldots\ldots\ldots\ldots\ldots\ldots\ldots 27$$

Multiplying equation 27 by aquifer thickness (h) equation 28 was obtained;

$$T_6 = 8\times10^{-6}h^2e^{-(0.0013\rho)} \quad \text{..... 28}$$

The plot (Figure 25) shows a strong linear correlation between transmissivity and transverse resistance (Equation 29) with a correlation coefficient of 0.9711.

$$T = 0.17R - 319 \quad \text{..... 29}$$

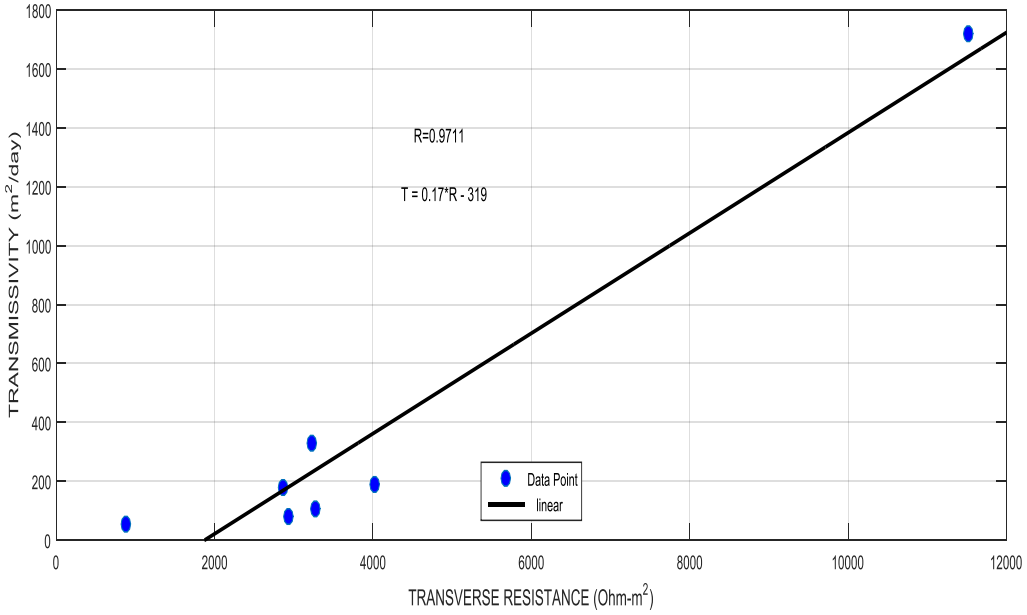

Figure 25: Plot of Transmissivity against Transverse resistance relative to geological formation of Basement Complex of Kaduna, Nigeria.

The transmissivity values (T_7) in table 5 shows values calculated using an experimental relation shown by equation 30 developed from measurements results for granitic area of central Finland (Jorma, 2012). The relation compares transmissivity with transverse resistance (R), this was directly applied to the data obtained for Matuu groundwater

potential zone and a strong correlation was realized (0.9734), however, the values of transmissivity realized were relatively low.

$$T = 0.00075R + 0.44 \quad \text{..... 30}$$

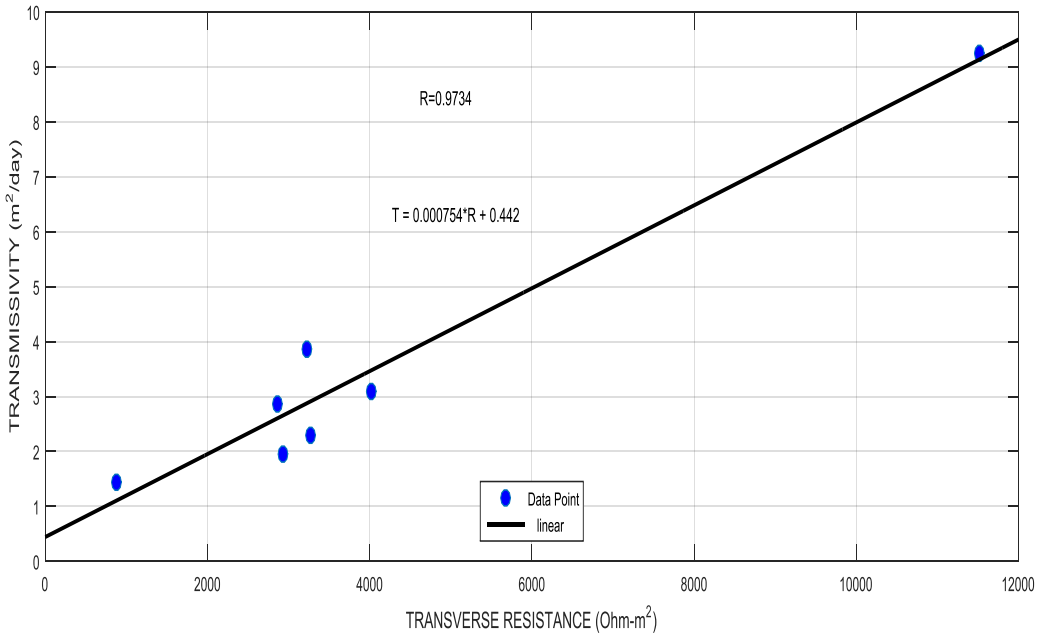

Figure 26: Plot of Transmissivity against Transverse resistance relative to geological formation of Central Finland.

Table 5 shows list of soundings of H-Type curve and the corresponding transverse resistance (R), thicknesses (h) and calculated transmissivity values (T_i) based on selected researches discussed earlier in this section mainly from similar geological settings to that of Matuu-Kilango area. T_i are the corresponding transmissivity values expressed in m^2/day, where i ranges from 1 to 7 for customized reference to case studies.

The names in bracket are the case study areas from which the used relations were obtained.

Table 5: Calculated Transmissivity Values for Matuu-Kilango area

VES	R (Ωm^2)	(h)	T (m^2/day) (Names in bracket are fields from which the used equations were developed)						
			T_1 (Oban Massif)	T_2 (Goa)	T_3 (Kabatini)	T_4 (Ondo State)	T_5 (Sinai)	T_6 (Kaduna)	T_7 (Central Finland)
YS1	11523.12	56.4	767	4648.41	736.16	11.83	13358.45	1719.71	9.259
YS2	3275.93	13.9	680	932.98	667.81	2.37	2087.78	108.47	2.282
YS5	4023.946	18.9	785	1617.53	749.75	4.14	4862.97	191.62	3.103
YS6	2867.9	17.5	557	796.14	561.61	2.22	1087.31	181.34	2.873
YS7	880.02	8.8	270.2	-43.43	216.89	0.56	118.72	51.92	1.445
YS8	3224.7	23.5	551	1044.31	556.07	2.94	1383.40	327.86	3.858
YS9	2935.598	11.9	707	855.24	689.54	2.16	2081.70	78.57	1.954

Table 6 shows results of transmissivity values as well as calculated transverse resistance values generated using an empirical relationship between transmissivity and transverse resistance (Equation 31) derived for phreatic aquifers of Deccan Trap Basalts, Godavari-Purna (Muralidharan & Shakar, 1996). The table displays high values of estimated transmissivity associated with relatively higher supply potentials of aquifers.

$$T = R^{0.678} \times 5.45 \quad \text{..... 31}$$

Table 6: Transmissivity estimations relative to Phreatic Aquifers of Deccan

VES	R (Ωm^2)	(h)	T (m^2/day)
YS1	11523.12	56.4	3091.3
YS2	3275.93	13.9	1317.6
YS5	4023.946	18.9	1514.8
YS6	2867.9	17.5	1203.9
YS7	880.02	8.8	540.5
YS8	3224.7	23.5	1303.6
YS9	2935.598	11.9	1223.2

A plot of Transmissivity (T) against Transverse resistance (R) yielded a linear relationship shown by equation 32 with a strong correlation coefficient of 0.9934 as shown in figure 27. The linear relationship depicted a relatively higher value of transmissivity even at zero transverse resistance.

$$T = 0.23 * R + 520 \quad \text{..... 32}$$

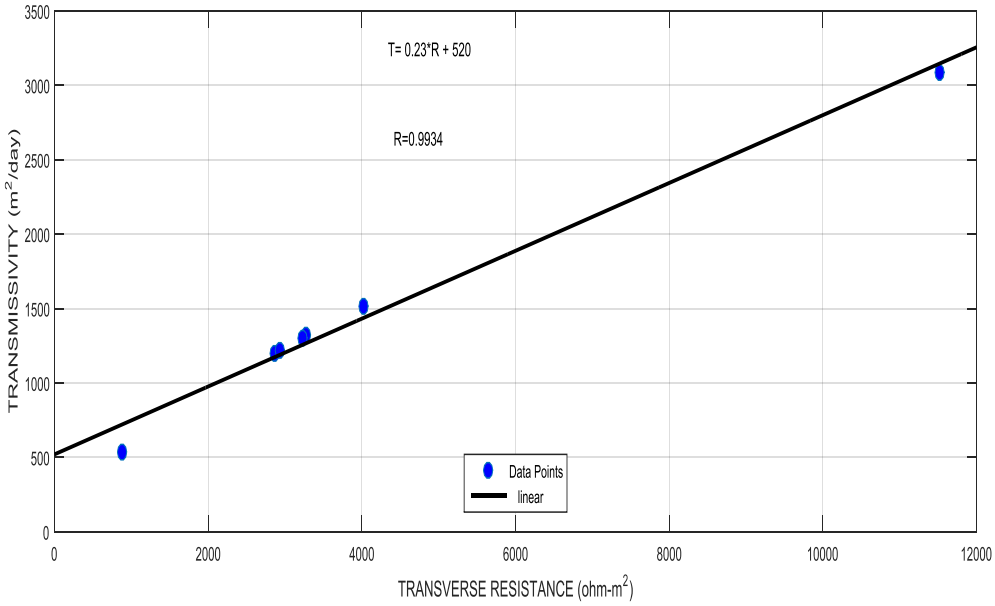

Figure 27: Plot Transmissivity against Transverse resistance relative to geological formation of Deccan Trap Phreatic Basalts, Purna.

From the results obtained in all the eight case study areas, two aspects of comparison were considered, i.e. cases with relatively strong correlation coefficients as well as similar geological formation as that of Matuu. This consideration narrowed down to two cases, that is, Ondo State, Southwestern Nigeria and Central Finland, (Table 7). The table displays findings of the work done at the case study areas, study interest and geological formation relative to the outcome for Matuu-Kilango area. The results associated with the two case studies were comparatively used to estimate transmissivity values for Matuu. The estimated result shows an average transmissivity of about 10 m^2/day, which is an indication of intermediate aquifer yield.

Table 7: Comparative analysis of case studies with similar charecteristics as Matuu

Case Study Area/Field	Ondo State, SouthWestern Nigeria (Mogaji et al., 2011)	Central Finland (Jorma, 2012)
Geological Formation	Fractured and faulted basement rocks made of granite gneiss, biotites gneiss, quartzite and Charnokite	2555.4 square kilometer granitic, other areas defined by mica gneiss among other crystalline magmatic units
Study Interest	Geophysical evaluation of rock type impact on aquifer characterization in hard rock terrain areas of Ondo State.	Investigation of hydraulic properties and drilled well yield with respect to factors related to well location in the Precambrian crystalline bedrocks of Central Finland.
Result summary for the case study area	Estimated average hydraulic conductivity for the aquifer units are 4.43, 0.96 and 4.58 m/day, while their mean transmissivity values are 13.0, 8.71 and 60.18 m^2/day respectively. Magmatites and Pegmatites were associated with confined aquifers with varying degree of fracturing while zones of minimal fracturing linked to biotites gneiss formations.	Yields are directly affected by topography and geological factors such as rock types and associated fault regimes. The median hydraulic parameters were found to be as follows: Transmissivity; $7.3x10^{-6}$ m^2/s, Hydraulic conductivity; $1.1x10^{-7}$ m/s, and Normalized yield; 12 $Lhr^{-1}m^{-1}$.
Range of Transmissivity values for Matuu, relative to case study area	0.56 m^2/day-11.83 m^2/day	1.445 m^2/day-9.259 m^2/day
Aquifer classification based on calculated transmissivity ranges for Matuu	Up to class III, Intermediate yield, (Withdrawals for local water supply)	Class IV, Low yield, (Smaller withdrawals for local water supply)
Correlation coefficient between Transmissivity and Transverse resistance for Matuu relative to the case study areas	0.9957 (Strong Correlation)	0.9734 (Strong Correlation)

3.9 Conceptual model

The research concepts outlined in this section was put into a pictorial illustration and a conceptual model shown in figure 28 was developed using Surfer 10 software, with an aim of providing a quick impression of subsurface setting of the study area associated to groundwater potential. The model (not to scale) provides a quick summary of the discussed findings of this research.

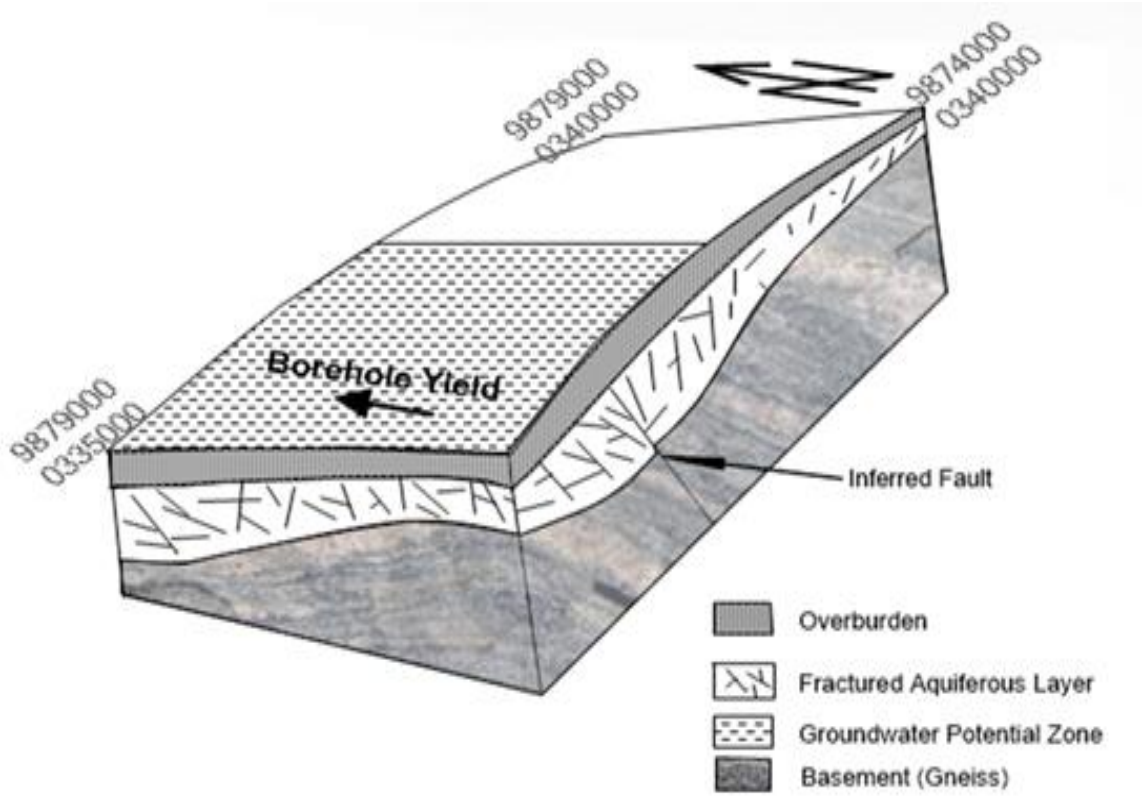

Figure 28: Conceptual model of subsurface formations associated with groundwater potential in Matuu-Kilango area.

CHAPTER FOUR

CONCLUSIONS AND RECOMMENDATIONS

4.1 Conclusions

Integrated inferences from magnetic anomaly trends, Euler deconvolution, self-potential trends, Wenner array and vertical electrical soundings conducted over Matuu-Kilango area has been used to conclude that west of Matuu-Kilango area is a groundwater potential zone based on findings of this on the delineated primers and the inferred aquifer at the zone. Boreholes sited at the west of study area will relatively register greater percentage of success good yields especially towards the north of the study area.

4.1.1 Groundwater Primers

Groundwater potential indicators (primers) were identified. This was evident from what was observed from electrical self-potential ranges, delineated faults and fractures, identified low resistivity layer, geo-electrical parameter trends and transmissivity attributes over the study area. Conclusions on each of the primers are stated on the subsequent sections.

4.1.1.1 Electrical Self-Potential Range

Recorded range of electrical self-potential values between -10mV to about -100mV in the western region of Matuu suggests presence of groundwater in the subsurface (Figure 17). The range agree with theoretically accepted values indicating groundwater potential discussed in chapter one section 1.6.2.1

4.1.1.2 Faults and Fractures

The area being underlain by crystalline hard rock system, the presence of groundwater can only be as a result of secondary porosity by faulting and fracturing. These faults were delineated by Euler-deconvolution technique where with a structural index of 0.5 the depth of the fractured zone was found to be 100 m from the surface. Considering the clustering of solutions and position of disjointed formation in profile BB', pronounced discontinuity along profile CC' and DD', it can be inferred that a fault exist in the western part of Matuu-Kilango area oriented in the SE-NW direction. This is surrounded by numerous fractures responsible for percolation and accumulation of groundwater associated with negative self-potential values obtained in this study. Towards the North-Western part of the study area, the depth to the structures slightly increases (from about 100 m to 150 m) indicating an increasing thickness of faulted layer of the subsurface thus greater potential for groundwater accumulation; this is a key groundwater primer.

4.1.1.3 Low Resistivity Layer

Wenner plot (r=50 m) showed anomalous low resistivity zone (≈130 Ωm) stretching from NW to South of study area, indicating the investigated faulted/fractured zone. Results from vertical electrical soundings describes the study area to be of three to four geo-electric subsurface system with generally black top soil, loose/weathered Micaceous gneisses and Biotite gneiss or fresh hard gneiss basement system of which the weathered layer showed characteristics of an aquiferous zone, an evidence of an existing aquifer. Soundings YS9, YS8 and YS1 that existed along the anomalous zone, indicated by

analyzed Wenner result, show increasing thickness of low resistivity layer to the north i.e. 11.9 m, 23.6 m and 74.8 m respectively.

4.1.1.4 Geo-electric Parameter trend

Using the measured apparent resistivity values and aquifer thicknesses of the soundings over the survey area, soundings to the west of Matuu showed higher values of transverse resistances as well as longitudinal conductance compared to those on the eastern part, the higher the values the higher the potential for groundwater, equally, the calculated values of longitudinal conductance increases to the North i.e. 0.071684, 0.203885 and 0.306062 for soundings YS9, YS8 and YS1 that existed along the anomalous zone respectively thus useful indicators for aquifer characteristics.

4.1.1.5 Transmissivity Attributes

Six out of eight sites from which parameter relations were obtained gave values indicating high/very high groundwater yields i.e. above 100 m^2/day limit, when applied for the Matuu groundwater potential zone. Of the considered relations, 3 were theoretical, 4 experimental and 1 empirical case, from areas in Finland, Nigeria, India, Kenya and Egypt. These sites are of hard rock basement system. Specifically, the experimental relation from Central Finland as well as the theoretical relation from Ondo State, Southwestern Nigeria, gave relatively strong correlation, with granitic Gneiss, Biotite Gneiss, Quartzite and Chamokite as geological formations, which is a similar situation in Matuu, the aquifer characteristics can be confidently compared. Over 60% of the soundings which gave H-Type curves, considered in transmissivity calculations fall

in the west of Matuu-Kilango area. Linear relationships between transmissivity and transverse resistance over the area showed strong correlation with correlation coefficients ranging from 0.5725 to 0.9971. However, estimated results showed transmissivity attributes of West Matuu to be approximately 10 square meters per day which indicate moderate hydraulic transmissivity associated with intermediate aquifer yield that can support local supply.

Figure 29 shows integration of the above discussed primers over the study area; indicating areas within which the most applicable ranges of self-potential, low resistivity, relatively high transmissivity and aquifer thicknesses are located. The intersection of the areas, showed by the dashed boundary (Figure 29), gives the best zone for siting boreholes.

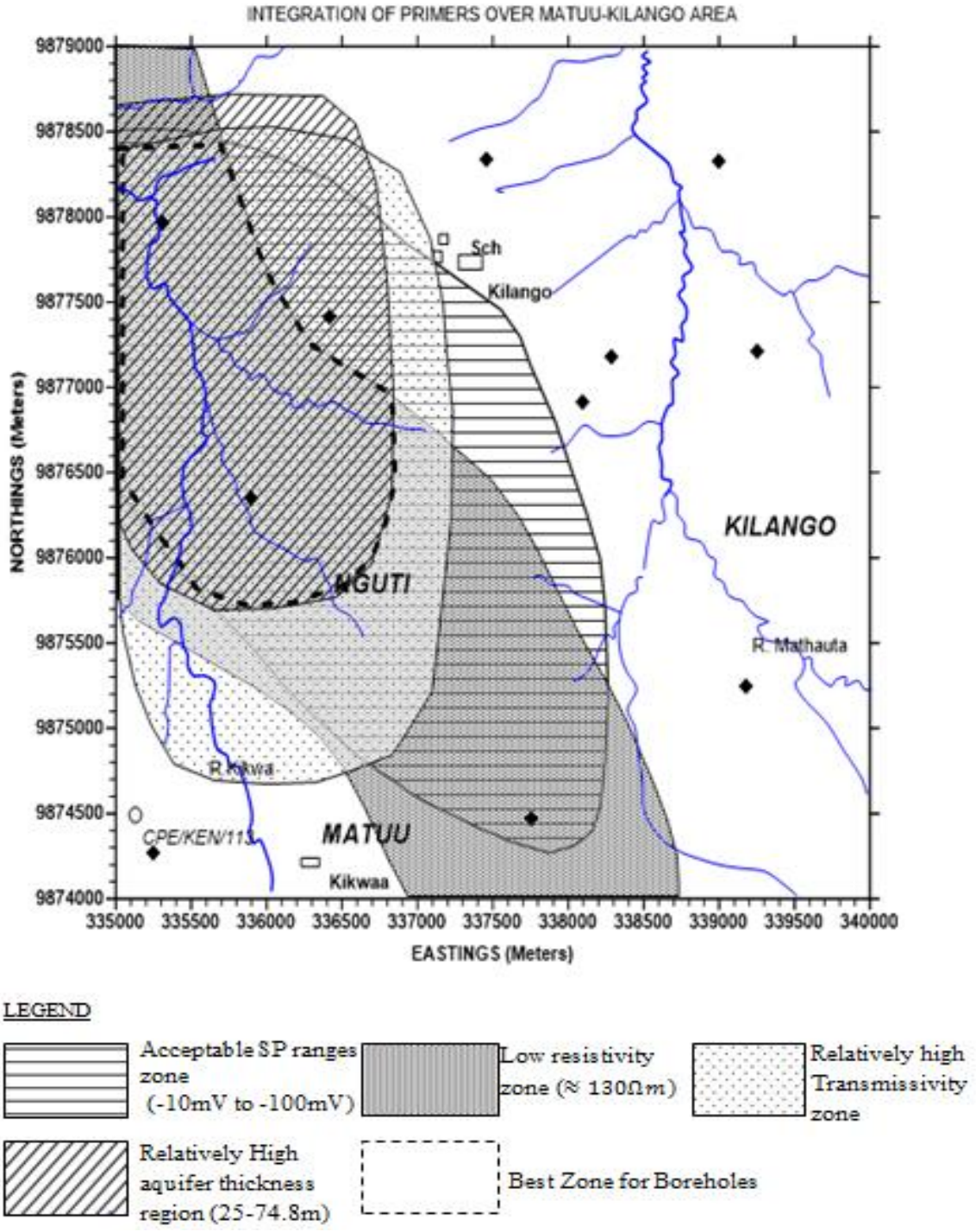

Figure 289: Map showing Integration of various Groundwater Primers over the study area

4.1.2 Aquifer Geometry

The inferred faulted aquifer is approximated to be located at the western part of the study area with average lateral stretch of 1500 m or greater if the western boundary of the study area is extended, and approximate depth of 100 m, with its thickness ranging from 10 m to about 80 m towards the North; an indication of best borehole yields in the North Western part of Matuu-Kilango area. This information forms a knowledge base for sustainable water development in Matuu-Kilango area.

4.1.3 The Model

A glance at the conceptual model reveal weathered layer location, variation in its thickness which is increasing to the North, the side of the study area with higher groundwater potential (western), resistive basement as well as overburden and the inferred fault.

4.2 Recommendations

More geophysical survey work needs to be done past the west of the study area to demarcate the extent of these subsurface features beyond the western boundary of the study area. Magnetic method employed in this survey gave general information on orientation of the inferred fault, a study involving square array resistivity technique is recommended to quantitatively investigate the fault orientation. As an attempt to confirm the survey result, it is recommended that exploratory wells be drilled. This can also make it possible to test expected borehole yields quantitatively over the zones proposed to have groundwater potential. Self-potential technique used in this research

delineated a conductive ore body at the central Matuu-Kilango area, a geotechnical or geological survey could be employed to map out this subsurface body.

REFERENCES

Afuwai, G., Lawal, K., Sule, P., & Ikpokotne, A. (2014). Geophysical Investigation of the causes of borehole failure in the Crystalline Basement Complex: A case study of Kaura area of Kaduna State, Nigeria. *Journal of Environment and Earth Science, 4*(23), 131-141.

Ahmed, S., Jayakumar, R., & Salih, A. (2008). *Groudwater Dynamics in Hard Rock Aquifers.* The Netherlands: Springer.

Amarachi, R., & Ako, B. (2012, April 22-25). *Groundwater Investigation using combined Geophysical methods*. Proceedings of the AAPG Annual Convention and Exhibition. Long Beach, California.

Anudu, G., Onuba, L. & Ufondu, L. (2011). Geo-electric sounding for Groundwater Exploration in the Crystalline Basement terrain around Onipe and adjoining areas: South Western Nigeria. *A Journal of Applied Technology in Environmental Sanitation, 1,* 38-54.

Baker, B. (1963). *Geology of Southern Machakos area.* Report geological Survey of Kenya 53. The Government Printer, Nairobi.

Bills, D., Truini, M., Flynn, M., Pierce, H., Catchings, R., & Rymer, M. (2000). Hydrogeology of the regional aquifer near Flagstaff, Arizona. *U.S Geological Survey and Water resources Investigations,* P. 143.

Chachadi, G. & Gawas, D. (2012). Correlation Study between Geoelectrical and Aquifer Parameters in West Coast Laterites. *International Journal of Earth Sciences and Engineering*, *5*(2), 282-287.

Cooper G. (2001). Euler (Version 1.00). [Mobile application software]. Johannesburg: School of Geosciences, University of Witwatersrand, South Africa.

Das, S., Mondal, N., & Singh, V. (2007). Groundwater Exploration in Hard Rock Areas of Vizianagaram District, Andhra Pradesh, India. *Jounal of Indian Geophysics Union*, *11*(2), 79-90.

Edet, A. & Okereke, C. (2015). *Hydrogeologic and hydrochemical framework of the shallow regolith aquifer, southern Oban massif (Nigeria).* Proceedings of the International Conference on Hard-Rock Aquifers: up-to-date Concepts and Practical Applications. La Roche Sur Yon.

Gangadhara T. (1992). Groundwater exploration techniques, *Lecture notes,* National Geophysical Research Institute.

Githiri, J., Patel, J., Barongo, J. & Karanja, P. (2011). Application of Euler Deconvolution Technique in determining depths to magnetic structures in Magadi Area, South Kenya Rift. *Journal of Agriculture Science and Technology, 13*(1), 142-156

Grauch, V., Hudson, R., Minor, A. & Caine, J. (2006). Sources of along-strike variation in magnetic anomalies related to intrasedimentary faults: A case study from the Rio Grande Rift, USA. *Exploration Geophysics, 37,* 372-378.

Harb, N., Haddad, K. & Farkh, S. (2010). Calculation of Transverse Resistance to correct aquifer resistivity of groundwater saturated zones: Implications for estimating its hydrogeological properties. *Lebanese Science Journal, 11*(1), 105-115.

Jinadasa, S. & Silva, R. (2009). Resistivity Imaging and Self-Potential applications in groundwater investigations in hard crystalline rocks. *Journal of the National Science Foundation of Sri Lanka*, *37*(1), 23-32.

Jiri, K. (1993). Classification of Transmissivity Magnitude and Variation. *Ground water, 31*(2), 230-236.

Jorma, M. (2012). *Drilled well yield and hydraulic properties in the Precambrian crystalline basement of Central Finland* (Ph.D. Thesis). University of Turku, Turku, Finland.

K'Orowe, M., Nyadawa, M., Singh, V., & Rangarajan, R. (2012). Geo-electric resistivity and groundwater flow models for characterization of hard rock aquifer system**,** *Global Advanced Research Journal of Physical and Applied Science, 1*(1), 12-31.

K'Orowe, M., Nyadawa, M., Singh, V., & Ratnakar D. (2011). Hydrogeophysical parameter estimation for aquifer characterisation in hard rock environments: A case study from Jangaon sub-watershed, India. *Journal of Oceanography and Marine Science, 2*(3), 50-62

Keary, P., Brooks, M. & Hill, I. (2002). *An Introduction to Geophysical Exploration*. London: Blackwell Scientific Publications.

Kudumnya, E., & Osumeje, J. (2015). Geo-electric investigation of the groundwater Potential distribution within the Northern Basement Complex of Nigeria. *International Journal of Scientific & Engineering Research, 6*(2), 1152-1160.

Kurniawan, A. (2009). Basic principles in using IPI2 Win Software. Retrieved from http://alvathea.wordpress.com.

Lateef, T. (2012). Geophysical Investigation for Groundwater Using Electrical Resistivity Method - A Case Study of Annunciation Grammar School, Ikere Lga, Ekiti State, South-Western Nigeria. *IOSR Journal of Applied Physic, 2*(1), 01-06.

MacDonald, A., Davis, J., & O'Dochartaigh, B. (2001). Simple methods for assessing groundwater resources in low permeability areas of Africa, *British Geological Survey Report* CR/01/168N.

Mansour, A. (2009). Geophysical Investigations for Groundwater in a complex subsurface terrain, Wadi Fatima, KSA: A case history. *Jordan Journal of Civil Engineering*, *3*(2), 118-136.

Mariita, N. (2009). Short Course IV on Exploration for Geothermal Resources, organized by UNU-GTP, GDC and KenGen. *The Magnetic Method*.Proceedings of a workshop, November 1-22 (pp. 1-8). Lake Naivasha, Kenya.

Mathu, E. (1992). The Mutito faults in the Pan-African Mozambique Belt, Eastern Kenya. In Mason R. (Ed.), *Basement Tectonics*. 61-69. Kluwer Academics Publishers, Netherlands.

Melinda, J., David, D., Michael, F., & Todd, T. (1997). Characterization of a Crystalline Rock aquifer near Lawrenceville, Georgia: *Application of Advances in borehole and Surface Geophysical methods*. Proceedings of Georgia Water Resources Conference, March 20-22 (pp. 369-372). The University of Georgia, Athens.

Mogaji, K., Olayanju, G., & Olalapo, M. (2011). Geophysical evaluation of rock type impact on aquifer characterization in the basement complex areas of Ondo State, Southwestern Nigeria: Geo-electric assessment and Geographic Information Systems (GIS) approach. *International Journal of Water Resources and Environmental Engineering*, *3*(4), 77-86.

Mosley, P. (1993). Geological Evolution of the Late Proterozoic Mozambique Belt of Kenya, *Tectonophys, 221*, 223-250.

Mulwa, J., Gaciri, S., Barongo, J., Opiyo-Akech, N. & Kianji G. (2005). Geological and Structural influence on Groundwater distribution and flow in Ngong area, Kenya. *African Journal of Science and Technology, Science and Engineering Series, 6*(1), 105-115.

Muralidharan, D. & Shankar, G. (1996). Relationship Between Electrical Transverse Resistance and Hydraulic Transmissivity of Phreatic Aquifers in Basalts. *Journal of Geological Society of India*. *47*, 33-36.

Murty, B., & Raghavan, V. (2002). The gravity method in groundwater exploration in crystalline rocks: a study in the peninsular granitic region of Hyderabad, India. *Hydrogeology Journal, 10*, 307-321.

Ndeto, R. (2011). *Water projects in Yatta District.* Projects brief reports WD/YAT/1/4/21. Tanathi Water Services Board, Kithimani, Kenya.

Nyamai, C., Mathu, E., Opiyo-Akech, N., & Wallbrecher E. (2003). A reappraisal of the geology, geochemistry, structures and tectonics of the Mozambique Belt in

Kenya: East of the Rift system. *African Journal of Science and Technology, Science and Engineering series, 4*(2), 51-71.

Nyamai, C., Opiyo-Akech, N., Gaciri, S., & Fujimaki H. (1999). Geochemistry and Tectonomagmatic Affinities of the Mozambique Belt and Intrusive rocks: a study in Matuu-Masinga Area, central Kenya. *Gondwana Research, 2*(3), 387-399.

Olorunfemi, M., & Fasuyi, S. (1993). Aquifer types and geoelectric/hydrogeologic characteristics of part of central basement terrain of Nigeria (Niger State). *Journal of Africa Earth Science, 16*(3), 309-317.

Pawan, D., Ramprasad, T., Ramana, M., Desa, M. & Shailaja, B. (2007). Automatic Interpretation of magnetic Data using Euler Deconvolution with Nonlinear Background. *Pure and Applied Geophysics, 164*, 2359-2372.

Reynolds, J. (1998). *An Introduction to Applied and Environmental Geophysics.* New York: John Wiley& Sons

Setyawan, A., Yudianto, H., Nishijima, J. & Hakim, S. (2015). *Horizontal Gradient Analysis for Gravity and Magnetic Data Beneath Gedongsongo Geothermal Manifestations, Ungaran, Indonesia*. Proceedings of World Geothermal Congress, April 19-25. Melbourne, Australia.

Sharma, S., & Baranwal, V. (2005). Delineation of groundwater-bearing fracture zones in a hard rock area: integrating Very Low Frequency electric and Resistivity data. *Journal of Applied Geophysics, 57*, 155-166.

Sosi, B., Cheboi, E., & Simiyu, C. (2013). Nonlinear Correlation analysis between Surface Resistivity and Hydraulic Characteristics of the Kabatini Well Field,

Upper Lake Nakuru Basin, Kenya Rift. *IOSR Journal of Applied Geology and Geophysics*, *1*(6), 35-45.

Survey of Kenya, (2005). *Topographical map of Matuu area*. Report Survey of Kenya 150/1. The government Printer, Nairobi.

Telford, W., Geldart, L. & Sheriff, R. (1990). *Applied Geophysics*. New York: Cambridge University Press.

Usama, M., Fernando, S., Mohamed, A., Ayman, T. & Abbas, M. (2010). Estimation of aquifer hydraulic parameters from surface geophysical measurements: a case study of the Upper Cretaceous aquifer, central Sinai, Egypt. *Hydrogeology Journal*, *18*, 699-710.

Utom, A., Odoh, B., & Okoro, A. (2012). Estimation of Aquifer Transmissivity Using Dar Zarrouk Parameters Derived from Surface Resistivity Measurements: A Case History from Parts of Enugu Town (Nigeria). *Journal of Water Resource and Protection*, *4*, 993-1000

William, L. (1966). *Geology of the Chanler's Fall area.* Report Geological Survey of Kenya 75. The Government Printer, Nairobi.

APPENDICES

Appendix 1: Raw Magnetic Data; Northing and Easting obtained by GPS and Average Reading from measured Total magnetic field values.

Profile 1		
Northing	**Easting**	**Reading**
9875000	340000	33927.05
9875200	340000	33837.65
9875400	340000	33613.9
9875600	340000	33492.4
9875800	340000	33789.5
9876000	340000	33779.85
9876200	340000	33685.4
9876400	340000	33607.15
9876600	340000	33578.2
9876800	340000	33936.9
9877000	340000	33664
9877200	340000	33609.55
9877400	340000	33613.6
9877600	340000	33570.3
9877800	340000	33689.25
9878000	340000	33778.65
9878200	340000	33684.85
9878400	340000	33664.15
9878600	340000	33734.1
9878800	340000	33630.75
9879000	340000	33625.4
9879200	340000	33660.35
9879400	340000	33764.35
9879600	340000	33790.4
9879800	340000	33747.8
9880000	340000	33672.35

Profile 2		
9875000	339000	33931.95
9875200	339000	33820.75
9875400	339000	33749.55
9875600	339000	33611.7
9875800	339000	33597.1
9876000	339000	33563.75
9876200	339000	33712.7
9876400	339000	33708.1
9876600	339000	33540.7
9876800	339000	33539.6
9877000	339000	33574.8
9877200	339000	33552
9877400	339000	33591.8
9877600	339000	33696.2
9877800	339000	33632.55
9878000	339000	33803.8
9878200	339000	33640.65
9878400	339000	33627.2
9878600	339000	33707.15
9878800	339000	33798.55
9879000	339000	33639.95
9879200	339000	33642.35
9879400	339000	33686.45
9879600	339000	33715.25
9879800	339000	33761.5
9880000	339000	33653.7

Profile 3		
9880000	338000	33681.75
9879800	338000	33789.9
9879600	338000	33723.75
9879400	338000	33604.35
9879200	338000	33671.1
9879000	338000	33731.05
9878800	338000	33573.9
9878600	338000	33597.85
9878400	338000	33678.8

9878200	338000	33689.95
9878000	338000	33716.7
9877800	338000	33686.4
9877600	338000	33665.6
9877400	338000	33671.25
9877200	338000	33380.5
9877000	338000	33426
9876800	338000	33622
9876600	338000	33682.5
9876400	338000	33430.5
9876200	338000	33229.5
9876000	338000	33576
9875800	338000	33679
9875600	338000	33538.25
9875400	338000	33768.3
9875200	338000	33941.05
9875000	338000	34002.9

Profile 4		
9875000	337000	34208.45
9875200	337000	34015.4
9875400	337000	33879.35
9875600	337000	33729.6
9875800	337000	33679.4
9876000	337000	33242.4
9876200	337000	33828.7
9876400	337000	33190.5
9876600	337000	33999.25
9876800	337000	34128.3
9877000	337000	34046.75
9877180	337000	33748.3
9877400	337000	33699.5
9877600	337000	33855.5
9877800	337000	33738.65
9878000	337000	33661.4
9878200	337000	33539.5
9878400	337000	33575.45
9878600	337000	33619.75
9878800	337000	33620.7
9879000	337000	33547.25
9879200	337000	33571.5
9879400	337000	33490.5
9879600	337000	33655.4
9879800	337000	33877
9880000	337000	33684.9

Profile 5		
9880000	336000	33600.4
9879800	336000	33611.65
9879600	336000	33423.3
9879400	336000	33590.3
9879200	336000	33589.5
9879000	336000	33584.7
9878800	336000	33569.35
9878600	336000	33601.45
9878400	336000	33683.65
9878200	336000	33792.5
9878000	336000	33721.05
9877800	336000	33835.45
9877600	336000	33933.9
9877400	336000	34085.35
9877200	336000	33894.85
9877000	336000	33402.7
9876800	336000	32971.15
9876600	336000	33101.65
9876400	336000	33104.25
9876200	336000	33415.05
9876000	336000	33565.4
9875800	336000	33659.15
9875600	336000	33665.2
9875400	336000	33788.85
9875200	336000	33866.85
9875000	336000	33975.4

Profile 6		
9880000	335000	33536.15
9879800	335000	33528.15
9879600	335000	33513.55
9879400	335000	33564.15

9879200	335000	33559.15
9879000	335000	33633.4
9878800	335000	33639.75
9878600	335000	33453.1
9878400	335000	33536.8
9878200	335000	33631.7
9878000	335000	33717.55
9877800	335000	33761.9
9877600	335000	33849.9
9877400	335000	33720.95
9877200	335000	33211.2
9877000	335000	32866.25
9876800	335000	33270.65
9876600	335000	33402.2
9876400	335000	33454.5
9876200	335000	33515.35
9876000	335000	33550.75
9875800	335000	33591.1
9875600	335000	33629.05
9875400	335000	33662.05
9875200	335000	33696.2
9875000	335000	33746

Short Profiles		
9877500	337000	33712.2
9877500	336900	33748.85
9877500	336800	33654.7
9877500	336700	33695.1
9877500	336600	33746.4

9877500	336500	33757.85
9877500	336400	33838.35
9877500	336300	33960.75
9877500	336200	33970.55
9877500	336100	34035.95
9877500	336000	34168.35
9878500	338000	33555.9
9878500	337900	33568.8
9878500	337800	33589.15
9878500	337700	33616.4
9878500	337600	33602.7
9878500	337500	33654.9
9878500	337400	33611.5
9878500	337300	33602.15
9878500	337200	33625.55
9878537	337100	33605.75
9878500	337000	33576.6
9875500	339000	33765.8
9875500	339100	33645.7
9875500	339200	33631.75
9875500	339300	33483.25
9875500	339400	33576.1
9875500	339500	33620.75
9875500	339600	33618.55
9875500	339700	33524.65
9875500	339800	33438.8
9875500	339900	33427.05
9875500	340000	33649.3

Appendix 2: Data obtained from Wenner Array resistivity measurement with constant separation of 50 meters.

NORTHING	EASTING	ELEVATION (meters)	ρ1 (Ωm)	ρ2 (Ωm)	AVARAGE (Ωm)
9874266	335251	1202	321.2	320.3	320.75
9877970	335307	1170	174.4	176.1	175.25
9876354.5	335891	1184	81.29	86.69	83.99
9877408.9	336413.3	1195	222.7	222.6	222.65
9878342.6	337459.9	1197	274.1	274.6	274.35
9874472.5	337758	1214	111.6	112.1	111.85
9876919.01	338099.08	1204	233.7	255.1	244.4
9877180.4	338289.24	1192	374.7	370.4	372.55
9878325.61	339001.49	1182	156.3	157.1	156.7
9875248.5	339182.7	1217	289.2	289.8	289.5
9877211	339254	1195	312.6	313	312.8

Appendix 3: Table of Data obtained from Vertical Electrical Sounding for 11 stations within Matuu-Kilango area.

YS1		YS2		YS3		YS4	
AB/2(m)	ρ(Avg)	AB/2(m)	ρ(Avg)	AB/2(m)	ρ(Avg)	AB/2(m)	ρ(Avg)
1.5	155	1.5	705.4	1.5	76.66	1.5	92.02
2	153.45	2	544.1	2	48.965	2	87.605
3	136.15	3	436.25	3	46.8	3	95.265
4	119.25	4	328.4	4	48.68	4	103.1
5	108.4	5	227.85	5	50.635	5	103.05
6	101.9	6	188.8	6	52.565	6	102.7
8	100.5	8	174.4	8	61.3	8	119.3
10	100.95	10	173.5	10	62.92	10	124.975
12	100.098	12	178.85	12	70.18	12	118.05
15	101.65	15	195.8	15	71.705	15	131.65
20	111.2	20	220	20	78.13	20	168.65
30	134.75	30	227.65	30	98.035	30	256.1
40	159.05	40	252.75	40	110.25	40	333.7
50	181.1	50	292.85	50	130.5	50	362.4
70	213.2	70	352.94	70	160	70	416.95
80	245.222	80	382.98	80	180.8	80	471.15

100	288.31	100	413.025	100	200.6	100	580.6
150	331.4	150	633.05	150	278.2		
		200	756	200	360.6		
YS5		**YS6**		**YS7**		**YS8**	
AB/2(m)	**ρ(Avg)**	**AB/2(m)**	**ρ(Avg)**	**AB/2(m)**	**ρ(Avg)**	**AB/2(m)**	**ρ(Avg)**
1.5	276.15	1.5	456.85	1.5	99.28	1.5	362.75
2	253.95	2	433.85	2	103.5	2	287.4
3	188.8	3	314.15	3	108.95	3	202.85
4	170	4	249.65	4	104.7	4	173.9
5	185.45	5	185.15	5	103.85	5	158.25
6	197	6	164.75	6	100.1	6	155.75
8	208.55	8	156.35	7	101.6	8	142.35
10	212.6	10	139.2	10	78.77	10	124.7
12	224.925	12	145	12	74.54	12	121.787 5
15	220.25	15	135.35	15	60.87	15	118.875
20	237.95	20	148.45	20	58.14	20	113.05
30	258.875	30	174.5	30	63.105	30	143.35
40	279.8	40	240.25	40	81.38	40	182.6
50	328.95	50	283.9	50	101.885	50	225.4
70	423.95	70	480.3	70	122.39	70	277.2
80	451.25	80	654.775	80	142.895	80	316.125
100	500.9	100	829.25	100	163.4	100	355.05
150	490	150	840.1	150	222.525	150	439.35
200	458.9			200	262.65	200	544.8
YS9		**YS10**		**YS11**			
AB/2(m)	**ρ(Avg)**	**AB/2(m)**	**ρ(Avg)**	**AB/2(m)**	**ρ(Avg)**		
1.5	627.85	1.5	4.468	1.5	66.75		
2	613.3	2	5.635	2	47.43		
3	436.95	3	7.654	3	46.955		
4	324.7	4	9.5345	4	52.075		
5	230.5	5	11.27	5	62.96		
6	217.025	6	13.415	6	70.485		
8	203.55	8	15.795	8	87.245		
10	198.75	10	19.1425	10	96.6975		
12	205.95	12	23.0425	12	105.53		
15	206.15	15	28.55	15	110.3		

20	240.5	20	37.62	20	118.5		
30	345.7	30	50.41	30	156.65		
40	410.45	40	64.31	40	183.25		
50	428.15	50	75.69	50	228.35		
70	500	70	102.67	70	284.8		
80	557.975	80	129.65	80	301.55		
100	615.95	100	155.35	100	402.05		
150	747.675	150	217	150	607.8		
200	879.4	200	265.95	200	701.9		